Int J Mech Mater Des (2022) 18:199–222
https://doi.org/10.1007/s10999-021-09570-w

Application of artificial intelligence to optimize the process parameters effects on tensile properties of Ti-6Al-4V fabricated by laser powder-bed fusion

Erfan Maleki · Sara Bagherifard · Mario Guagliano

Received: 21 April 2021 / Accepted: 7 October 2021 / Published online: 28 October 2021

Abstract Laser powder-bed fusion (LPBF) process, as one of the most widely used technologies of additive manufacturing, enables fabrication of parts with intricate geometries. The choice of process parameters in this technology plays a major role in defining the microstructural, mechanical and surface properties of the fabricated parts. In this study, the effects of LPBF process parameters on static tensile properties (including yield strength and ultimate tensile strength and elongation) of Ti-6Al-4V samples were investigated using artificial intelligence methods. Deep learning approach was employed by using neural networks for prediction, optimization and parametric and sensitivity analyses. Relevant experimental data available in the literature were collected to feed the network. Stacked auto-encoder was assigned to the networks for high accuracy pre-training. LPBF process parameters including laser power, scanning speed, hatch spacing, layer thickness and sample direction were regarded as inputs while yield strength, ultimate strength and elongation were considered as outputs of the neural networks. The obtained results indicate the high potential of neural networks to be used as a powerful tool for process parameter optimization for enhanced mechanical performance of additive manufactured parts.

Keywords Additive manufacturing · Mechanical properties · Optimization · Deep learning · Neural networks

E. Maleki (✉) · S. Bagherifard · M. Guagliano
Department of Mechanical Engineering, Politecnico di Milano, Milan, Italy
e-mail: erfan.maleki@polimi.it

S. Bagherifard
e-mail: sara.bagherifrad@polimi.it

M. Guagliano
e-mail: mario.guagliano@polimi.it

1 Introduction

Additive manufacturing (AM) has gained notable attention to enhance fabrication efficiency in a wide range of sectors including aviation, automotive, medical, etc. Complex geometries can be fabricated more efficiently using various AM technologies, compared to conventional subtractive manufacturing techniques or other forming methods such as rolling, casting, etc. (Gardan 2016; DebRoy et al. 2018).

During the last decades, several techniques have been developed for AM of metallic materials. Based on the ASTM F2792 standard, AM methods have been classified into two major categories of direct energy deposition (DED) and powder bed fusion (PBF) (ASTM International 2013). Main used technologies in both groups of DED and PBF for metals and alloys are presented in Table 1.

Moreover, some other alternative techniques including sheet lamination (SL) (Gu et al. 2012),

Table 1 Classification of the main AM processes for metals and alloys

AM process technologies	
DED	PBF
Direct metal deposition (DMD)	Selective laser sintering (SLS)
Laser engineered net shaping (LENS)	Direct metal laser sintering (DMLS)
Directed light fabrication (DLF)	Electron beam melting (EBM)
Wire and arc additive manufacturing (WAAM)	Selective laser melting (SLM)
Gas metal arc welding additive manufacturing (GMAW-AM)	
Laser cladding (LC)	

binder jetting (BJ) (Thompson et al. 2015), friction stir welding AM (FSW AM) (Sharma et al. 2017), cold spraying (CS) (Bagherifard et al. 2017, 2018, 2020; Bagherifard and Guagliano 2020; Ghelichi et al. 2014) direct metal writing (DMW) (Chen et al. 2017) and diode-based processes (DBP) (Matthews et al. 2017) are also suggested for metal AM of metallic materials.

Besides the beneficial features of AM, because of the layer-by-layer fabrication process and the complex physical phenomena during melting and solidification or fusion and bonding of the material (Yadroitsev and Smurov 2011), various types of defects can be generated on the surface and through the bulk of AM parts (Maleki et al. 2020a). These irregularities and defects are mainly created by overheating and unstable melting, vaporization and lack of fusion, attachment of partially melted powders, changes in chemical composition, thermal residual stresses, uncontrolled wetting and surface contaminants (DebRoy et al. 2018; Yakout et al. 2017,2018,2019; Nasab et al. 2018; Sames et al. 2016). These defects can negatively affect the mechanical properties of AM materials compared to the ones fabricated by conventional manufacturing processes (Yadollahi and Shamsaei 2017). Each AM technology is characterized and controlled by a set of particular parameters, the alteration of which directly affects the properties of the fabricated material. A notable effort has been recently put into experimental investigation of the role of individual process parameters for different AM techniques to obtain the optimal range for different classes of materials. Table 2 lists the experimental studies performed using different AM technologies on various types of metallic materials. These process parameters optimization was mostly carried out with the aim to modulate a specific physical or mechanical property such as porosity, yield and ultimate tensile strength, hardness and surface roughness.

Besides experimental studies, as presented in Table 3, other alternative methods of modelling and optimization such as finite element modelling (FEM), multi-objective accelerated process optimization (m-APO), response surface methodology (RSM), Taguchi method (TM), analysis of variance (ANOVA), genetic algorithm (GA), artificial neural network (ANN), recurrent neural network (RNN) and convolutional neural network (CNN) have also been used to analyse and optimize the process parameters of AM technologies. In addition, it should be mentioned that a comprehensive review study about applications of AI and machine learning in AM was performed by Wang et al. (Wang et al. 2020a). Also, some other studies based on analytical solutions were also suggested to investigate the effect of AM process parameters on tensile properties (Campoli et al. 2013; Choren et al. 2013) and residual stresses (Aggarangsi and Beuth 2006; Fergani et al. 2017).

Despite the vast number of studies performed in this field, there are still several issues to be addressed considering the quality and performance of AM metallic materials. Artificial intelligence (AI) based methods such as neural networks (NN) has demonstrated a remarkable capability in optimization in different fields of science and engineering (Maleki et al. 2017; Maleki and Unal 2019; Maleki and Farrahi 2018), and have been already used also in AM, as mentioned in Table 3. In general, a NN has three major layers of input, hidden and output (Maleki and Unal 2020a). Shallow neural network (SNN), as the primary generation of artificial neural networks mostly used in

Table 2 Experimental studies on the role of different AM process parameters on mechanical and physical properties

AM type	Technology	Feed-stock material	Reference
DED	DMD	Al/AlN	Riquelme et al. (2019)
	GMAW-AM	H08Mn2Si	Xiong et al. (2018)
	WAAM	S960	Liberini et al. (2017)
	DMD	AISI 304L	Wang et al. (2016)
	LENS	AISI H13	Wołosz et al. (2020)
PBF	SLS	WC–Co	Kumar and Czekanski (2017)
	DMLS	AlSi10Mg	Fathi et al. (2019)
	EBM	Ti-6Al-4V	Maizza et al. (2019)
	EBM	Ti-6Al-4V	Manjunath et al. (2020)
	EBM	Ti-6Al-4V	Ge et al. (2014)
	EBM	W	Yang et al. (2019a)
	EBM	Inconel 718	Ding et al. (2019)
	EBM	AISI 316L	Wang et al. (2018)
	SLM	Ti-6Al-4V	Cunningham et al. (2019)
	SLM	Ti-6Al-4V	Sun et al. (2019)
	SLM	Ti-6Al-4V	Baitimerov et al. (2017)
	SLM	Ti-6Al-4V	Qiu et al. 2013)
	SLM	AlSi10Mg	Yang et al. (2019b)
	SLM	AlSi10Mg	Kempen et al. (2011)
	SLM	AlSiMg0.75	Bai et al. (2018)
	SLM	CoCr	Tonelli et al. (2020)
	SLM	CoCrW	Wang et al. (2020b)
	SLM	Inconel 718	Gockel et al. (2019)
	SLM	Inconel 718	Moussaoui et al. (2018)
	SLM	Mg-Ca	Liu et al. (2017)
	SLM	Zr-1Mo	Sun et al. (2020)
	SLM	17–4 PH	Averyanova et al. (2012)
	SLM	18 Ni marage 300	Mutua et al. (2018)

simulation of different processes, has 1 or 2 hidden layers, which are generally trained by back-propagation (BP) algorithm (Maleki and Maleki 2015; Maleki et al. 2018, 2020b). The large number of data set required for SNN development, can be quite limiting (Livingstone et al. 1997). Considering the improvements achieved in NNs by deep learning methods including restricted Boltzmann machine (RBM) and deep belief network (DBN) presented by Hinton et al. (Hinton et al. 2006; Hinton and Salakhutdinov 2006), it is feasible to develop deep neural network (DNN) using greedy layer-wised pre-training with a smaller data set. Other alternative methods for pre-training of DNN such as stacked auto-encoder (SAE) were later presented, to make the development of DNN possible with small data set while achieving higher efficiency by increasing the number of hidden layers and using SAE in between them (Bengio et al. 2007; Feng et al. 2019; Liu et al. 2018; Bin Wang et al. 2017).

The studies on the application of ANNs for process parameters optimization of different AM technologies, as presented in Table 3, used mainly SNNs. Deep learning was only employed in the studies, which considered RNN and CNN. Herein, we investigate the application of deep learning method by using NNs on LPBF process parameters' optimization for fabrication of Ti-6Al-4V parts based on the experimental data available in the literature. NN modelling was carried out by developing different SNN, DNN and stacked auto-encoder assigned deep (SADNN) neural networks to analyze and optimize the process parameters' effects on yield strength and ultimate tensile strength and elongation of LPBF fabricated Ti-6Al-4V parts. Figure 1 illustrates the methodology used in this study

Table 3 Numerical and analytical studies on the role of different AM process parameters on mechanical and physical properties

Modelling or optimization methods	AM Technology	Feed-stock material	Output parameter	Reference
FEM	SLM	Inconel 625	Surface roughness	Zheng et al. (2019)
	EBM	Inconel 718	Grain morphology	Raghavan et al. (2016)
	SLM	AlSi10Mg	Fatigue life	Schnabel et al. (2019)
	LENS	AISI 304L	Plastic strain	Stender et al. (2018)
m-APO	SLM	Ti-6Al-4V	Relative density Elongation	Aboutaleb et al. (2019)
RSM	SLS	Ti	Total area of sintering	Paul and Anand (2012)
TM	SLM	AISI 316L	Surface roughness	Campanelli et al. (2013)
	SLM	Ti-6Al-4V	Relative density	Alfaify et al. (2018)
	SLM	Ti-6Al-4V	Density	Sun et al. (2013)
	SLM	VV751P	Ultimate strength	Khaimovich et al. (2018)
ANOVA	SLM	Ti-6Al-4V	Relative density	Malỳ et al. (2019)
	SLM	Ti-6Al-4V	Porosity	Hassanin et al. (2016)
	SLM	Ti-6Al-4V	Young modulus Tensile strength Ultimate strength Elongation	Zhang et al. (2019a)
	SLM	18 Ni marage 300	Relative density	Casalino et al. (2015)
	SLM	Cu–Cr–Zr	Density	Ma et al. (2020)
	SLS	Ni	Porosity	Liao and Shie (2007)
	LC	P420	Cladding width	Saqiba et al. (2014)
GA	SLM	Al	Bead width	Garg et al. (2014)
ANN	SLM	Al	Bead width	Garg et al. (2014)
	LC	P420	Cladding width	Saqiba et al. (2014)
	SLS	AISI 316L	Porosity	Marrey et al. (2019)
	GMAW-AM	Cu coated steel	Bead width Bead height	Xiong et al. (2014)
	DMD	Ti	Porosity	Zhang et al. (2019b)
RNN	DED	AISI 316L	Thermal history	Mozaffar et al. (2018)
CNN	SLM	Ti-6Al–4V AlSi10Mg Inconel 718 AISI 316L 17–4 PH	Surface quality	Scime and Beuth (2018)
	SLM	AISI 316	Melt-pool classification	Kwon et al. (2018)

for process parameters optimization of Ti-6Al-4V fabricated by LPBF.

2 Collected data from literature

In this study, the experimental data available in literature for Ti-6Al-4V parts fabricated via LPBF technology were collected to feed the NNs. In the LPBF process, parts are fabricated by successive layer by layer laser beam irradiation to a powder bed, selectively melting the powders to create a melt pool. Afterward, by quick cooling and solidification of the molten pool the part is progressively constructed layer by layer (Thijs et al. 2010). A series of process parameters have been recognized to significantly

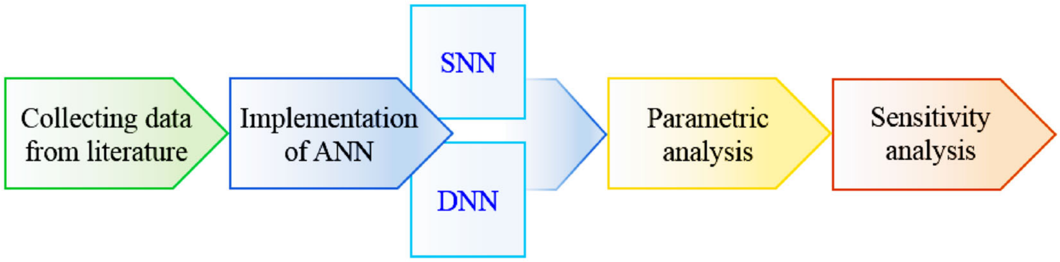

Fig. 1 Schematic illustration of the methodology used in this study for process parameters optimization of Ti-6Al-4V fabricated by LPBF

affect the quality and properties of the LPBF material. Laser power, laser diameter, scanning speed, hatch spacing, thickness of the melted layer and building direction as well as power density E (described in Eq. 1) can be considered as the major controlling parameters (Cardaropoli et al. 2012):

$$E = p/vht \tag{1}$$

where p is the laser power, v is the scanning speed, h is the hatch spacing and t is the thickness of melted layer.

Due to the high cooling rate, as-built LPBF Ti-6Al-4V parts exhibit mostly fine α'-martensite microstructure (Wu et al. 2016; Cain et al. 2015). The yield and ultimate tensile strength of the as-built parts are generally higher than those of materials produced by conventional manufacturing methods; however, due to the low ductility of α'-martensite, these parts are characterized by lower elongation and ductility (Edwards and Ramulu 2014; Simonelli et al. 2014; Vilaro et al. 2011). In addition to the microstructural characteristics, the selection of LPBF process parameters controls also the risk to generate defects, voids and surface irregularities, which can remarkably affect the mechanical properties of as-built material. Figure 2 provides some examples to illustrate the effects of variation of LPBF parameters on the quality of as-built Ti-6Al-4V in terms of porosity and surface morphology.

Considering laser power, scanning speed, hatch spacing, thickness of melted layer and the angle between building direction and sample main axis as input parameters and yield strength, ultimate tensile strength and elongation as output parameters, the collected data from the literature are presented in Table 4. From the data provided in the 3rd column in Table 4, it can be observed that the powders have a wide particle size distribution; therefore, due to this high scatter, the effects of powder particle size are not considered as input for developing NNs. Figure 3 depicts the morphology of Ti-6Al-4V feedstock powder used for LPBF technology, highlighting the wide variation.

3 Developed neural networks

NNs are inspired from performance and capability of human's brain in understanding problems and presenting logical solutions by means of functional relations. These networks can be used for modeling and analysis of complex and non-linear processes with several variable factors (Maleki et al. 2019). Schematic architecture of a single layer NN fed with r and s number of input (p) and output (a) parameters, with correspondent weight matrixes (w), bias vectors (b), linear combiner (u) and transfer function (f), is presented in Fig. 4a. Among 52 datasets collected from the literature, 42 cases (80%) were considered for training and 10 cases (20%) were regarded to assess the obtained network structures. A random selection strategy was followed for the data used in training and testing processes. Performance and accuracy of the networks was evaluated through calculating the correlation coefficient (R^2) described as follows (Tetko et al. 1995):

$$R^2 = \frac{\sum_{i=1}^{n}\left(f_{EXP,i} - F_{EXP}\right)\left(f_{ANN,i} - F_{ANN}\right)}{\sqrt{\sum_{i=1}^{n}\left(\left(f_{EXP,i} - F_{EXP}\right)^2\left(f_{ANN,i} - F_{ANN}\right)^2\right)}} \tag{2}$$

where, n is the number of fed samples, and f_{EXP} and f_{ANN} represent the experimental and predicted values, respectively. F_{EXP} and F_{ANN} are determined as described below:

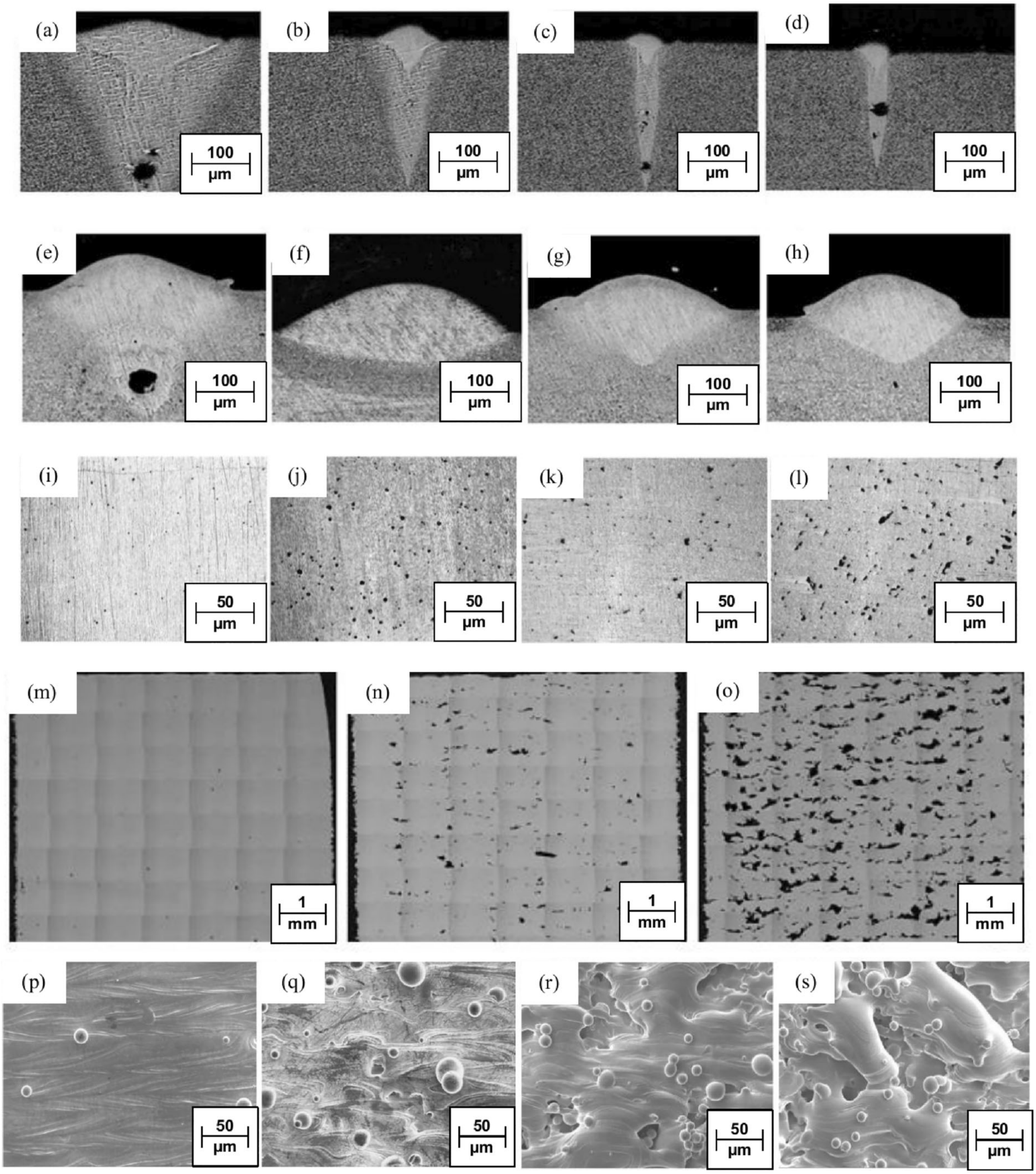

$$F_{EXP} = \frac{1}{n}\sum_{i=1}^{n} f_{EXP,i} \tag{3}$$

$$F_{ANN} = \frac{1}{n}\sum_{i=1}^{n} f_{ANN,i} \tag{4}$$

The flowchart of the methodology followed in this study is presented in Fig. 4b. Different SNNs and DNNs were developed by trial and error to obtain high performance NN. Main LPBF process parameters as described before were considered as inputs and tensile

◀**Fig. 2** Representative images illustrating the effects of SLM process parameters including laser power *p*, laser beam diameter *d*, scanning speed *v*, hatch spacing *h*, thickness of melted layer *t*, and energy density *E* on the quality of as-built LPBF fabricated Ti-6Al-4V. Cross-sectional optical micrographs of single scan track produced with different beam diameters and speeds of **a** *d = 50* µm, *p = 400* W, *v = 25* mm/s, **b** *d = 50* µm, *p = 400* W, *v = 50* mm/s, **c** *d = 50* µm, *p = 400* W, *v = 75* mm/s, **d** *d = 50* µm, *p = 400* W, *v = 100* mm/s, **e** *d = 200* µm, *p = 400* W, *v = 25* mm/s, **f** *d = 200* µm, *p = 400* W, *v = 50* mm/s, **g** *d = 200* µm, *p = 400* W, *v = 75* mm/s and **h** *d = 200* µm, *p = 400* W, *v = 100 mm/s* adopted from (Shi et al. 2018). Optical micrographs of as built Ti-6Al-4V fabricated with different energy densities of **i** *E = 74* J/mm^3, **j** *E = 100* J/mm^3, **k** *E = 32* J/mm^3 and **l** *E = 27* J/mm^3 adopted from (Gong et al. 2015). Variation of Ti-6Al-4V porosity with different thicknesses of melted layer **m** *t = 20 µm, p = 400 W, v = 2400 mm/s*, **n** *t = 60 µm, p = 400 W, v = 2400 mm/s* and **o** *t = 100* µm, *p = 400* W, *v = 2400* mm/s adopted from (Qiu et al. 2015). Surface morphologies of fabricated material with different thicknesses of melted layer and scanning speed **p** *t =* 20 µm, *p = 400* W, *v = 2300* mm/s, **q** *t = 20* µm, *p = 400 W, v = 3500* mm/s, **r** *t = 60* µm, *p = 400 W, v = 2400* mm/s and **s** *t = 80* µm, *p = 400* W, *v =* 2400 mm/s adopted from (Qiu et al. 2015)

test properties of the fabricated Ti-6Al-4V material were regarded as outputs assigned to the developed NNs.

Figure 4c reveals a typical SNN with two hidden layers. Besides the number of layers in a NN, the number of neurons acting as computational nodes is one of the major variable parameters of the network structure. Oftentimes, increasing the number of neurons can improve the performance of the NN, although it increases the computational costs (Maleki et al. 2021). Figure 4d provides a schematic illustration of the architecture of a DDN, which is basically a modified SNN with more hidden layers. DNNs can be developed with or without pre-training process. In Fig. 4d, SAE is assigned to DNN for pre-training. SAE is assigned in between the layers of DNN. Therefore to construct SADNN with *j* layers and full inter-connection, *j-1* SAEs are required and for the presented model with a total of 6 layers consisting of: input layer + 4 hidden layers + output layer, 5 SAEs were utilized. Considering the number of layers and neurons, 6 layers SADNN with 6 + (15 + 12 + 9 + 6) + 3 structure, has 5 SAEs, with 6 + (15) + 6, 15 + (12) + 15, 12 + (9) + 12, 9 + (6) + 9, 6 + (3) + 6 structures.

Assignment of SAEs to DNNs according to the number of neurons in each layer of DNN is shown in the right part of Fig. 4d. The number of neurons in each SAE is similar to the ones used in the corresponding DNN layer. First the SAE catches the input fed to DNN as its own inputs and outputs data; after processing them the outputs in its hidden layer are transferred to the second SAE as the new input. This process continues up to a point when it reaches the last SAE. After successfully training all SAEs, the obtained initial weight and bias values of each layer $w^j(0)$, are assigned to DNN's corresponding layer to initialize the modelling process with fine-tuned SADNN.

After identifying the optimum structure of NN with the highest performance, chain rules based on the values of weights and biases are implemented to determine the model functionality considering the results obtained in all the layers, as described below:

$$a^1 = f^1\left(w^1 i + b^1\right) \tag{5}$$

$$a^2 = f^2\left(w^2 i^1 + b^2\right) \tag{6}$$

$$a^3 = f^3\left(w^3 i^2 + b^3\right) \tag{7}$$

$$a^4 = f^4\left(w^4 i^3 + b^4\right) \tag{8}$$

$$a^5 = f^5\left(w^5 i^4 + b^5\right) \tag{9}$$

$$\begin{aligned} a^6 &= M(m(1), m(2), m(3)) = f^6\left(w^6 i^5 + b^6\right) \\ &= f^6(w^6 f^5(w^5 f^4(w^4 f^3(w^3 f^2\left(w^2 f^1\left(w^1 i + b^1\right) + b^2\right) \\ &\quad + b^3) + b^4) + b^5) + b^6) \end{aligned} \tag{10}$$

where a^1, a^2, a^3, a^4 and a^5 are the outputs of the first to fifth layers, respectively. Function *M* assigns the values of the 6 considered input parameters of laser power, scanning speed, hatch spacing, thickness of melted layer and sample direction to the 3 output parameters of yield strength *m(1)*, ultimate tensile strength *m(2)* and elongation *m(3)*.

Finally, to specify the relative impact of each input parameter on the outputs, a sensitivity analysis is carried out by means of the obtained weight matrix of NN and Garson equation as follows (Olden et al. 2004; Maleki and Unal 2020b):

Table 4 Collected data from the available literature for LPBF fabricated Ti-6Al-4V

Reference No	Data sample No	Powder size (μm)	SLM parameters						Measured properties		
			Laser power (W)	Scanning speed (mm/s)	Hatch spacing (μm)	Sample direction* (°)	Thickness of melted layer (μm)	Energy density (J/mm^3)	Yield strength (MPa)	Ultimate tensile strength (MPa)	Elongation (%)
Zhao et al. (2019)	1	15–45	170	800	80	90	30	510	1025	1210	7.8
Tao et al. (2018)	2	23–56	280	1200	140	0	30	980	1025	1305	8.7
	3	23–56	280	1200	140	90	30	980	1180	1310	6.8
Vilaro et al. (2011)	4	20–55	160	600	200	0	40	2133.33	1137	1206	7.6
	5	20–55	160	600	200	90	40	2133.33	962	1166	1.7
Mertens et al. (2014)	6	25–50	175	710	120	90	30	887.32	1166	1321	2.0
He et al. (2019)	7	10–50	135	800	75	45	30	379.68	1142	1235	1.3
Yang et al. (2017)	8	15–53	200	1500	75	90	30	300	1054	1098	6.1
Gong et al. (2015)	9	17–44	120	960	100	0	30	375	1098	1237	8.8
	10	17–44	120	540	100	0	30	666.66	1150	1257	8.0
	11	17–44	120	400	100	0	30	900	1066	1148	5.4
	12	17–44	120	1260	100	0	30	285.71	932	1112	6.6
	13	17–44	120	1500	100	0	30	240	813	978	3.7
Zhao et al. (2016)	14	26–51	200	1000	100	0	50	1000	1200	1300	7.5
	15	26–51	200	1000	100	90	50	1000	1160	1240	7.1
Yang et al. (2016)	16	20–50	500	400	70	45	40	3500	1130	1340	5.8
	17	20–50	200	400	70	45	40	1400	1055	1320	4.4
Stef et al. (2018)	18	7–18	41.7	400	70	90	30	218.92	1000	1220	1.85
Voisin et al. (2018)	19	10–45	250	1600	70	0	30	328.12	1140	1290	7.6
	20	10–45	100	800	84	90	30	315	1110	1305	8.6
Shi et al. (2017)	21	25–55	310	1100	180	90	60	3043.63	1020	1098	10.2
	22	25–55	310	1100	180	0	60	3043.63	1050	1163	14.1
Yu et al. (2017)	23	15–70	200	1000	80	0	20	320	915	1150	7.6
	24	15–70	200	1000	80	90	20	320	1045	1270	6.2
Cai et al. (2018)	25	20–60	200	600	160	0	50	2666.66	1110	1195	8.2
Zafari et al. (2019)	26	15–45	200	900	105	0	30	700	1150	1220	6.1
	27	15–45	200	1100	105	0	30	572.72	1150	1190	14.5
	28	15–45	200	786	105	0	30	801.52	1130	1175	12.1
	29	15–45	200	688	105	0	30	915.69	1105	1155	12.4
Yang et al. (2019c)	30	20–44	280	1200	120	90	30	840	1110	1225	9.8
Cao et al. (2018)	31	16–50	280	1200	140	0	30	980	1040	1200	9.6

Table 4 continued

Reference No	Data sample No	Powder size (µm)	SLM parameters						Measured properties		
			Laser power (W)	Scanning speed (mm/s)	Hatch spacing (µm)	Sample direction* (°)	Thickness of melted layer (µm)	Energy density (J/mm^3)	Yield strength (MPa)	Ultimate tensile strength (MPa)	Elongation (%)
Zhang et al. (2019c)	32	20–53	400	1000	100	0	60	2400	810	977	4.8
Simonelli et al. (2014)	33	18–40	194	800	120	0	20	582	805	1000	3.9
	34	18–40	194	1000	80	0	20	310.4	815	1020	4.2
	35	18–40	194	600	70	0	20	452.66	900	1075	4.7
	36	18–40	194	400	90	0	20	873	920	1085	6.1
	37	18–40	194	800	120	90	20	582	810	1060	3.8
	38	18–40	194	1000	80	90	20	310.4	900	1090	4
	39	18–40	194	600	70	90	20	452.66	1040	1210	4.3
	49	18–40	194	400	90	90	20	873	1060	1260	5.1
Xu et al. (2015)	41	25–45	175	710	120	0	30	887.32	950	1095	9.1
	42	25–45	375	1029	120	0	60	2623.90	1065	1225	11.5
	43	25–45	375	686	120	0	90	5903.79	980	1120	0.9
Pang et al. (2019)	44	20–44	280	1000	120	90	30	1008	1050	1410	5.3
	45	20–44	280	1200	120	90	30	840	1100	1480	4.2
	46	20–44	280	1400	120	90	30	720	1030	1390	4.7
	47	20–44	280	1600	120	90	30	630	1010	1200	5.5
	48	20–44	280	1200	120	0	30	840	910	1100	4.5
	49	20–44	280	1200	120	30	30	840	1020	1310	4.2
	50	20–44	280	1200	120	45	30	840	1170	1300	4.0
	51	20–44	280	1200	120	60	30	840	1180	1310	5.5
Zhang et al. (2018)	52	20–40	170	1250	100	0	30	408	1084	1262	6.1

*Sample direction zero corresponds to the vertical build up direction

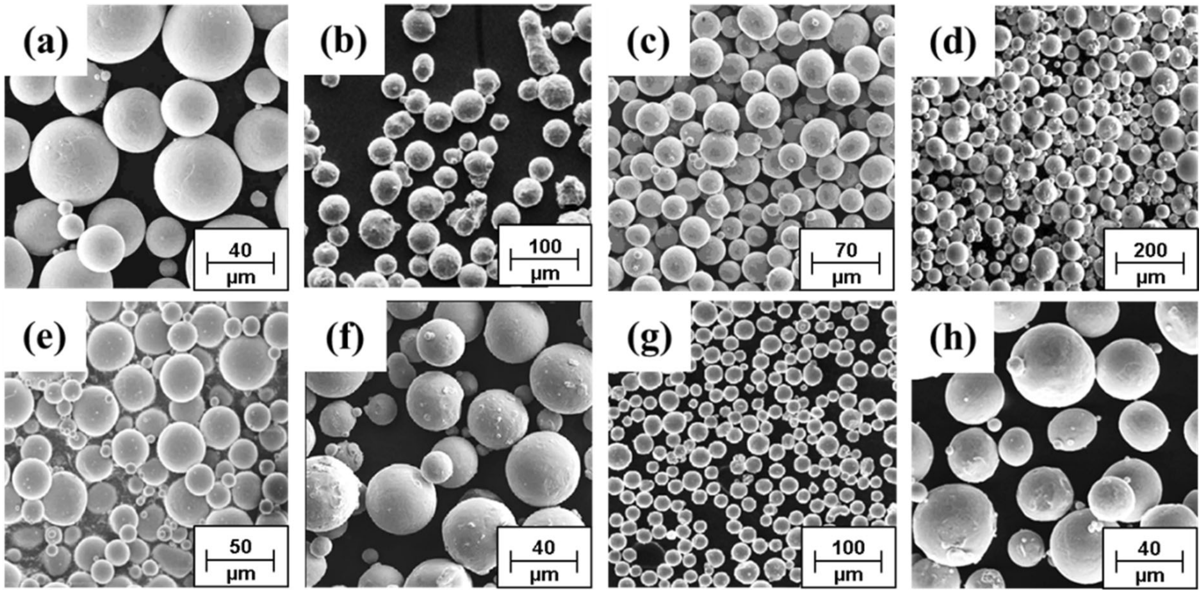

Fig. 3 Morphologies and particle size distribution of Ti-6Al-4V feed-stock powder used in LPBF processes **a** 10–50 μm adopted from (He et al. 2019), **b** 26–51 μm adopted from (Zhao et al. 2016), **c** 25–55 μm adopted from (Shi et al. 2017), **d** 15–70 μm adopted from (Yu et al. 2017), **e** 20–44 μm adopted from (Yang et al. 2019c), **f** 16–50 μm adopted from (Cao et al. 2018), **g** 18–40 μm adopted from (Simonelli et al. 2014) and **h** 20–40 μm adopted from (Zhang et al. 2018)

$$I_j = \frac{\sum_{m=1}^{N_h}\left(\left(\frac{\left|W_{jm}^{ih}\right|}{\sum_{k=1}^{N_i}\left|W_{km}^{ih}\right|}\right) \times \left|W_{mn}^{ho}\right|\right)}{\sum_{k=1}^{N_i}\left\{\sum_{m=1}^{N_h}\left(\frac{\left|W_{km}^{ih}\right|}{\sum_{k=1}^{N_i}\left|W_{km}^{ih}\right|}\right) \times \left|W_{mn}^{ho}\right|\right\}} \tag{11}$$

where I_j is the importance of jth input parameter relevant to the output parameter, N_i and N_h are the numbers of input and hidden neurons, respectively, and W is the connection weight; the superscripts i, h, and o in turn refer to input, hidden and output neurons.

4 Results and discussion

To achieve a NN structure of high performance and compare the efficiency of SNN, DNN and SADNN, several networks with different architecture and network parameters were developed. Accuracy of the results in terms of output parameter of yield strength obtained from SNNs with 1 and 2 hidden layers as a function of neurons' number is shown in Fig. 5a. It can be observed that increasing the number of neurons, notably enhances the performance of the SNN network.

Figure 5b compares the accuracy of the estimated yield strength using SNNs, DNNs and SADNNs. In all cases, 6 and 3 neurons were respectively used for input and output layers, considering a learning rate of 0.195 and a Logarithmic-Sigmod transfer function. The results indicate that SADNN with a structure of $6 + (15 + 12 + 9 + 6) + 3$ exhibited the highest performance among all the developed NNs, showing accuracies of 0.99 and 0.98 for training and testing processes, respectively. The details of the developed network performance evaluation are presented in Table 5. In order to investigate the performance independency of the obtained optimum structure from the used data fed to the network, three more orders of data set were generated using random function to select the data for training and testing (42 samples for training and 10 samples for testing). Performance evaluations of the other randomly selected data are shown in Table 6. It can be observed that in the whole considered randomly derived data sets, like the one already used, accuracies of at least 0.99 and 0.98 were obtained for training and testing processes, respectively.

In this study, high prediction accuracy for tensile properties such as elongation was obtained which is usually highly fluctuated particularly for the LPBF samples due to unforeseen processing defects by using a relatively small dataset. This point can be

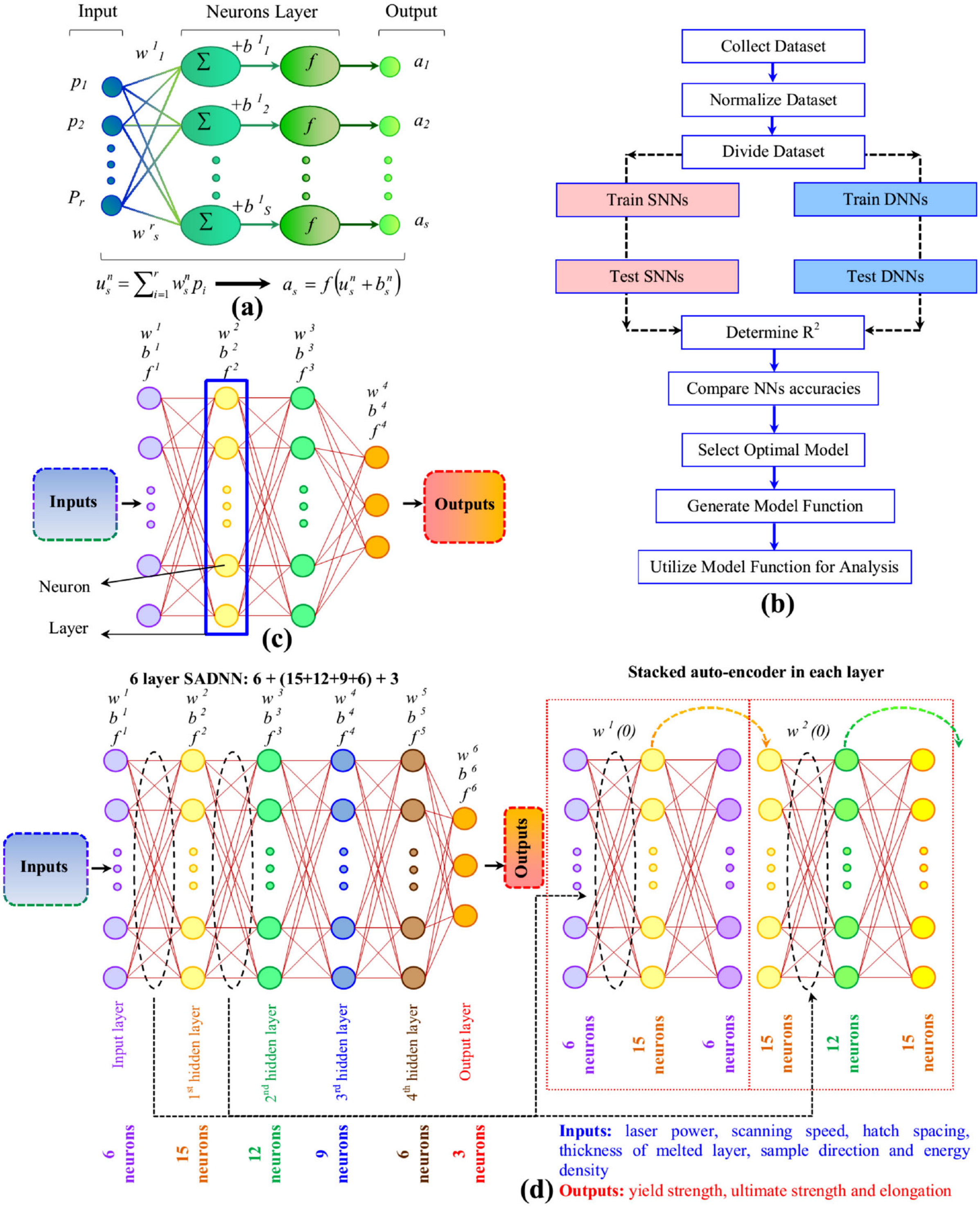

Fig. 4 **a** Schematic illustration of structure of a NN with one hidden layer considering the weight matrixes *w*, bias vectors *b*, linear combiner *u* and transfer function *f*. **b** The flowchart describing the approach used in this study considering R^2 value as an index of predicted results' accuracy. **c** Schematic representation of a SNN with 2 hidden layers. **d** The architecture of the developed 6 layers DNN and SADNN models considering assignment of SAE to SADNN

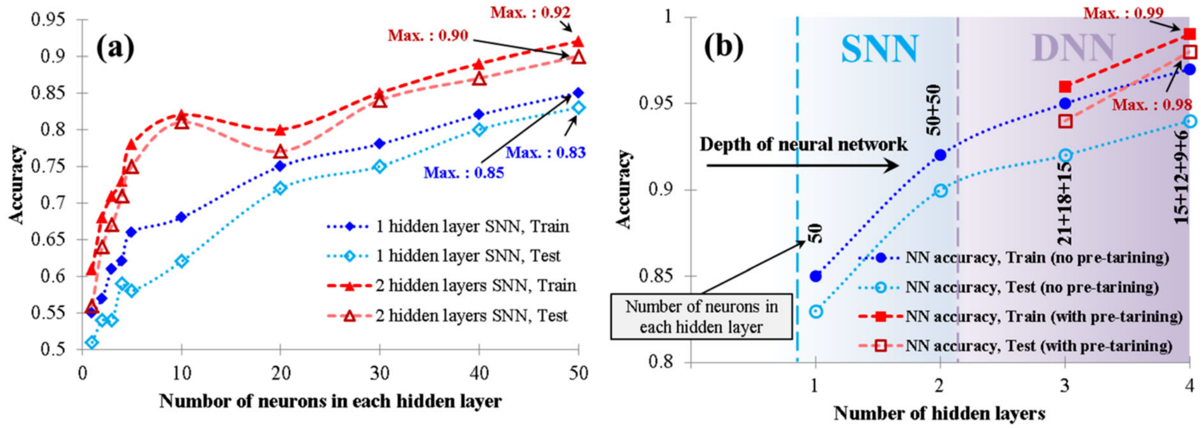

Fig. 5 **a** The effects of number of neurons in each layer of SNNs vs. accuracy of yield strength estimation. **b** Comparison of the yield strength estimation accuracy between developed NNs of different structures

investigated with two different aspects. Firstly, in this study, as all major parameters of LPBF process including laser power, scanning speed, hatch spacing, layer thickness and sample direction were considered as inputs, the whole process is modeled completely. Variations of the mentioned input parameters affect the states of the fabricated LPBF materials in terms of internal (such as porosities resulted by entrapment of inert gas in the melt pool during the melting of powder or keyhole pores or lack of fusion discontinuity) and surface (such as surface morphology) properties which directly affect the tensile behaviors such as elongation of the material. In addition, considering the feed-stock material, same material was investigated and only the effects of powders size were neglected due to their high scattering in each performed experiment. Secondly, as the main novelty of this study, it was found that, stacked auto-encoder as a pre-training tool can play a critical role to increase the accuracy of the modeling developed by a small set of data.

Table 5 R^2 values for individual output parameters in both training and testing phases obtained using SADNN

Output parameter	Obtained R^2	
	Training	Testing
Yield strength	0.9932	0.9887
Ultimate strength	0.9956	0.9921
Elongation	0.9944	0.9917

Having validated the high performance of the developed SADNN, model function was generated for parametric analysis of LPBF process to evaluate the contribution of each process paramter to the tensile properties of Ti-6Al-4V samples. For the paramteric analysis, based on the available experimental data, the following intervals were considred for each input paramter: 42 W $\leq$ laser power $\leq$ 500 W, 70 µm $\leq$ hatch spacing $\leq$ 200 µm, 20 µm $\leq$ thickness of melted layer $\leq$ 90 µm and 0 $\leq$ sample direction $\leq$ 90°.

The results of the parametric analysis in terms of yield strength, ultimate tensile strength and elongation are presented in Figs. 6, 7 and 8, respectively. According to the obtained results, the variation of LPBF procerss paramters affects the considered outputs in a various ways directly correlated with the role of the corresponding parameter in the build up formation.

As shown in Figs. 6a and 7a, high scanning speed and low laser power lead to the lack of fusion and poor adhesion, and thus result in very low yield and ultimate strengths, as confirmed by experimental studies (Yakout et al. 2019; Mutua et al. 2018; Tran and Lo 2019); Fig. 8a shows a similar trend for elonagtion. For high power and scanning speed > 600 mm/s, due to the exposure to temperatures higher than boiling temperature of Ti-6Al-4V and evaporation, the fabricated material becomes distorted leading to extremely low yield and ultimate tensile strengths (Tran and Lo 2019; Yan et al. 2018). Experimental

Table 6 R^2 values for individual output parameters in both training and testing steps obtained by SADNN in the three different orders of randomly selected data

Randomly selected data set	Output parameter	Obtained R^2	
		Training	Testing
Data set 1	Yield strength	0.9911	0.9853
	Ultimate strength	0.9907	0.9879
	Elongation	0.9962	0.9927
Data set 2	Yield strength	0.9909	0.9916
	Ultimate strength	0.9934	0.9909
	Elongation	0.9944	0.9921
Data set 3	Yield strength	0.9957	0.9902
	Ultimate strength	0.9912	0.9889
	Elongation	0.9924	0.9931

studies have evidenced that in the area representing high power (> 200 W) and low speed, due to the overheating and unsatbale melting, keyhole melting phenomena can occur leading to the formation of gas-induced defects and large spherical pores (Tran and Lo 2019; Le et al. 2019; Meier et al. 2018). These pores will negatively affect the mehchanical properties of the LPBF fabricated material (Choo et al. 2019). As illustrated in Fig. 8a, in the high power (> 300 W) and low scanning speed (< 500 mm/s) regime, the induced high energy density can activate the keyhole mechanism that will result in notable reduction of elongation.

In the LPBF process, hatch spacing can directly affect the heat-transfer and extent of overlap in the scanning direction (Tran and Lo 2018; Xia et al. 2016), as well as the relative density and build-up rate (Qiu et al. 2015; Su and Yang 2012). Increased hatch spacing upto unfavorable ranges will reduce the maximum temperature and heat accumulation; this will result in reduced melt pool width leading to inadequate melting of the particles, and decreased density of the part (Dong et al. 2018; Aboulkhair et al. 2014). As it can be observed in Figs. 6b and 7b, in the area correponding to high hatch spacings (> 150 µm) due to the increased porosity of material, yield and ultimate tensile strengths are quite low. Also, in the low hatch spacing ($\approx$70–100 µm) and high scanning speeds ($\approx$900–1600 mm/s) zones, due to the insufficient melting of powders, the yield and ultimate tensile strengths are reduced. However, the obtained results for elongation (Fig. 8b) reveal that high elonagtion can be achieved, whithin the ranges of 140–200 µm and 1000–1600 mm/s for hatch spacing and scanning speed, respectively.

The thickness of the melted layer, as one of the main parameters of the LPBF process, can directly affect the building rate and fabrication efficiency. This parameter also influences the heat and mass transfer as well as cooling rate whithin the melt pool. These aspects can control the tensile properties of the LPBF fabricated materials. For high thicknesses, the generated energy density might not be enough to fully melt the powder layer and thus balling phenomenon could occur. Thereore, the insueffícnt bonding could be obtained between powders and the underlying material, resulting also in lower density (Zhang et al. 2013; Guan et al. 2013; Olakanmi et al. 2015). This phenomenon can be observed in Figs. 6c and 7c, in the regimes corresponding to layer thicknesses > 50 µm, where the yield and ultimate strengths are reduced. Considering that the final properties of the material is controlled by the synergistic effect of all process paramters, in the high layer thicknesses regime, if favorable scanning speeds are used, higher elongation can be obtained for the fabricated material. For instnace, it has been reported that for SLM fabricated 1Cr18Ni9Ti stainless steel samples, the elongation enhanced by increasing the layer thickness from 100 to 150 µm while setting the scanning speeds in the high range of 2000–4000 mm/s; however the yield and ultimate strengths were reported to be decreased for these samples (Ma et al. 2015). Herein, Fig. 8c, shows that the elongation of the LPBF fabricated Ti-6Al-4V samples is increased by rising layer thickness whithin the range of 30–90 µm and scanning speeds in the range of

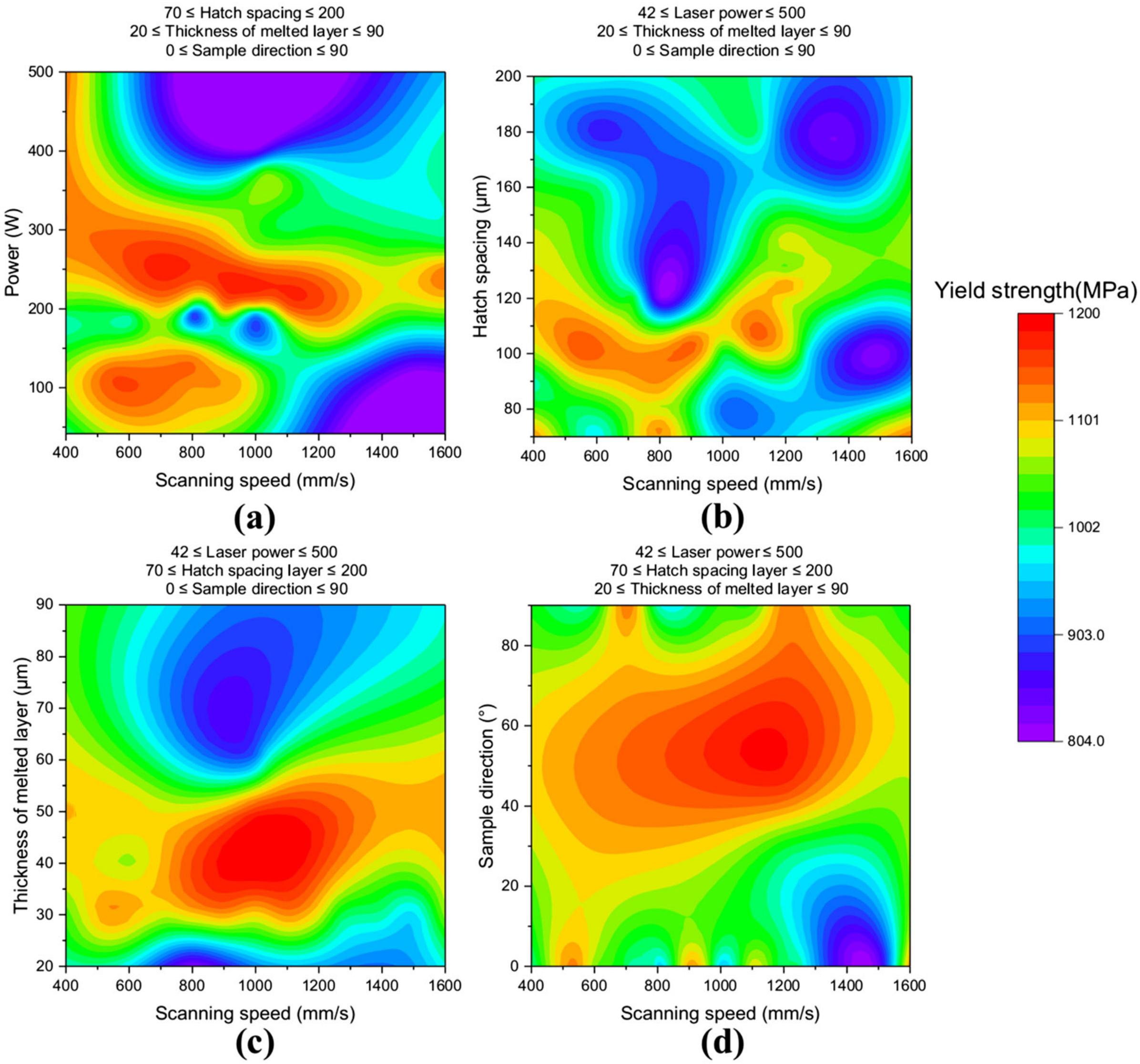

Fig. 6 Parametric analysis of the effects of LPBF process parameters on yield strength of Ti-6Al-4V in terms of **a** laser power and scanning speed, **b** hatch spacing and scanning speed, **c** thickness of melted layer and scanning speed and **d** sample direction and scanning speed

1000–1600 mm/s; however, the elongation is very low in areas with thicknesses > 40 µm and scanning speeds < 1000 mm/s.

Sample direction in terms of the relative angle between the longitudinal axis of the sample and the considerded building direction is another important parameter known to affect the properties of LPBF fabricated material. As also reported in Table 4, in most of the experiments in the field, parts have been fabricated either vertically or horizentally with sample directions of 0° and 90°, respectively (considering z axis parallel to the building direction). Adjusting this parameter is quite challenging as besides its dependancy on other process paramters, it is very sensitive to the powder type in trerms of material and morphological aspects. It was reported that while keeping all LPBF process parameters constant, parts fabricated with larger size powders demonstrate lower yield and ultimate strengths progressively when built along 0°, 45° and 90° directions; however, the effect of

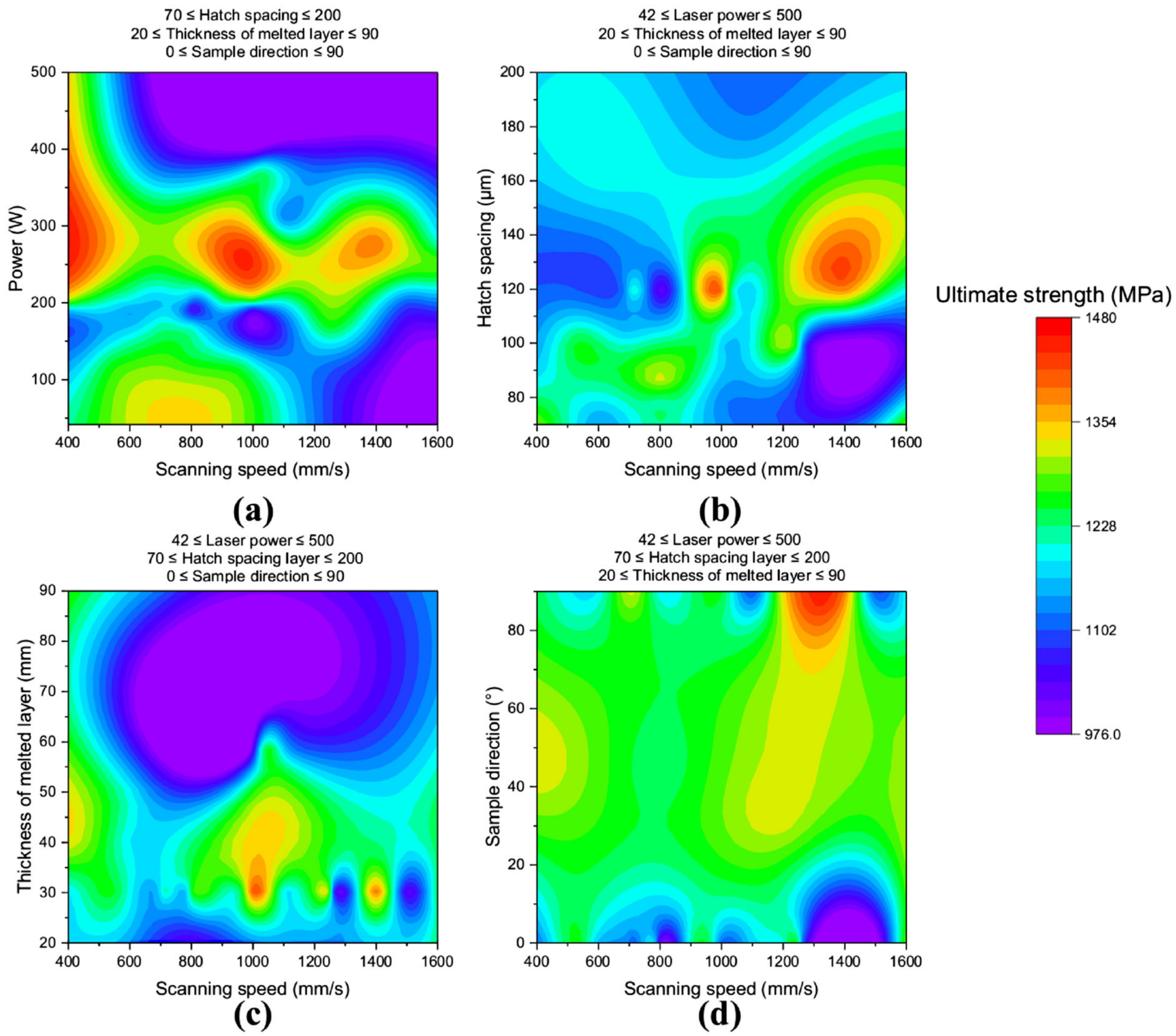

Fig. 7 Parametric analysis of the effects of LPBF process parameters on ultimate tensile strength of Ti-6Al-4V in terms of **a** laser power and scanning speed, **b** hatch spacing and scanning speed, **c** thickness of melted layer and scanning speed and **d** sample direction and scanning speed

orientation is on elongation follows a trend cotrary to yield and ultimate tensile strength (Spierings et al. 2011). As mentioned before, in this study the effects of powder size and morphology were not considered in the NN modelling, due to the high scatter of the available experimental data. Furthermore, due to the quality of the bonding and the bundaries of solidified material in the layer-by-layer fabrication, the yield and ultimate stngths are reduced and elongation is increased for 0° (vertically built sample) compared to 90° sample dirtection (horizentally built sample) (Guan et al. 2013; Buchbinder et al. 2011; Sui et al. 2019). The results obtained in terms of sample direction and scanning speed indicate that sample directions whithin 40–90° lead to higher yield and ultimate strengths compared to other build-directions (see Figs. 6d and 7d). On the other hand, as shown in Fig. 8d, in most cases the elogation is higher in lower angles of build-direction in particular for 0° in the scanning speed ranges of 700–800 and 900–1200 mm/s. Also, in the higher angle sample directions of about 75–90° and scanning speeds of 1000–1200 mm/s, the elonagtion is in midlevel and quasi high.

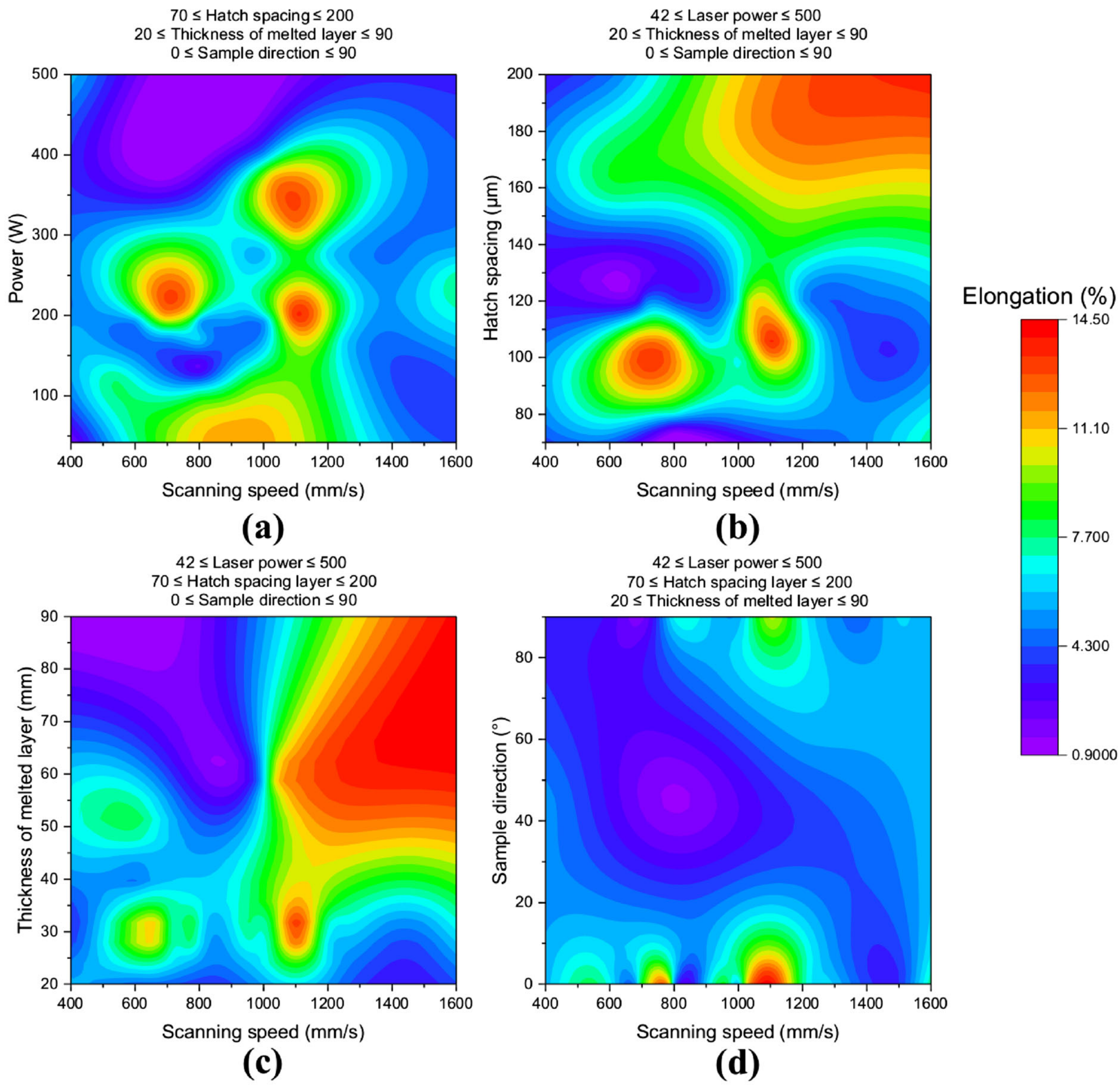

Fig. 8 Parametric analysis of the effects of LPBF process parameters on elongation of Ti-6Al-4V in terms of **a** laser power and scanning speed, **b** hatch spacing and scanning speed, **c** thickness of melted layer and scanning speed and **d** sample direction and scanning speed

Parametric analysis were performed for prediction of yiled strength, ultimate tensile strength and elonagtion in terms of energy density and sample build-direction as depicted in Fig. 9. The effects of laser power, scanning speed, hatch spacing and layer thickness are included in energy density. The results indicate that for high energy densities and low angle sample dirctions, lower yield and ultimate tensile strengths can be obtained due to the insuefficent melting (see Fig. 9a and b). However, for energy densities < 4500 J/mm^3 and sample dirction angles > 30°, higher yield and tensile ultimate strengths can be reached. Also for energy densities of about 1000–2000 J/mm^3 and sample directions angles of 70–90°, yield and ultimate tensile strengths can reach to their highest values. However, as presented in Fig. 9c, different behavoir is obtianed for elonagtion in terms of energy denisty and sample

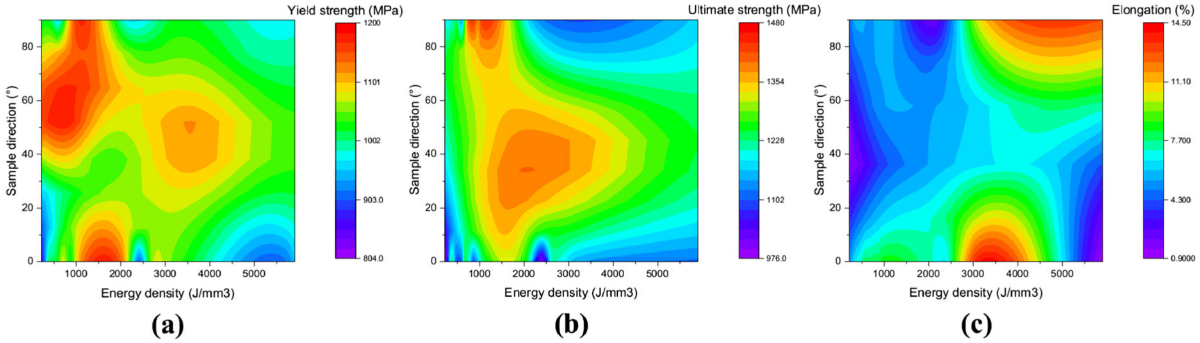

Fig. 9. 2D contours representing the effect of energy density and sample direction on tensile mechanical properties of LPBF fabricated Ti-6Al-4V **a** yield strength, **b** ultimate strength and **c** elongation

direction. High elonagtion can be obtained in two different areas: in the region corresponding to energiy density of 2700–4500 J/mm^3 and sample direction angle of 0–20°, and also in the region of energy density of 3000–5900 J/mm^3 and sample direction angle of 70–90°.

Figure 10 illustrates the results obtained from sensitivity analysis. The analysis confirms that all the considered input parameters for the developed SADNN, directly affect the tensile properties of LPBF fabricated Ti-6Al-4V material. Ranks of importance of each input on outputs parameters are shown in Fig. 9 to highlight the effectiveness of the variation of different input parameters on the outputs.

Yield and ultimate tensile strengths were found to be more sensitive to the scanning speed, laser power, hatch spacing, layer thickness and sample direction, in a progressive order. However regarding elongation, laser power and scanning speed have the most importance, hatch spacing and layer thickness have equal effects in the 3rd rank and sample direction has the least significant effect. These results reveal that for instance to achieve higher tensile strength, variation of scanning speed and laser power can be more effective compared to other parameters.

Based on the obtained results, it can be observed that the developed NN model can play crucial role for LPBF process parameters optimization for fabrication of Ti-6Al-4V parts. As it mentioned (in introduction), mostly AM process parameters optimization has been carried out by design of experiment and the relevant experimental characterizations which are often costly

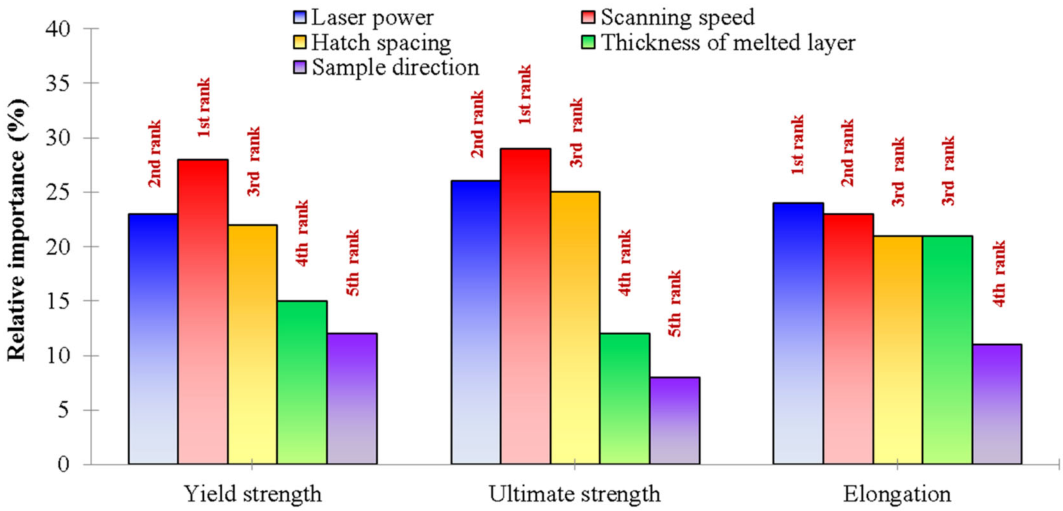

Fig. 10 Sensitivity analysis data on the tensile properties of LPBF fabricated Ti-6Al-4V

in terms of time and money. In addition, novel experiments in this field which are based on trial-and-error approach are time consuming and exorbitant in particular for metal AM (Wang et al. 2018,2019; Sun et al. 2016). Therefore, using AI based systems such as NNs for optimization of AM process parameters for different materials can pave a path to reduce the extra costs by eliminating successive experiments. In development of the NN based models, rather than the process parameters and characteristics of the feedstock material, the effects of used equipment as well as scanning strategies can be considered in upcoming studies.

5 Conclusion

In this study neural networks were used to investigate the effects of laser powder-bed fusion process parameters on the mechanical tensile properties of Ti-6Al-4V. Combination of deep learning and stacked auto-encoder was used for prediction, and optimization as well as parametric and sensitivity analyses using neural networks. Different neural networks including shallow neural network, deep neural network and stacked auto-encoder assigned deep neural network were developed and evaluated in terms of their efficiency. An extensive review was performed to collect all the relative experimental data available in the literature on Ti-6Al-4V to feed the developed networks. The main parameters of laser powder-bed fusion process including laser power, scanning speed, hatch spacing, layer thickness and sample direction were considered as inputs and yield strength, ultimate tensile strength and elongation were regarded as outputs of the neural networks. Comparing the accuracy of the obtained outputs of the developed networks indicated that pre-trained stacked auto-encoder assigned deep neural network exhibited the highest performance; thus this network was used for further analysis. The results also indicated that increasing the depth of the neural network in terms of number of layers could play an important role in enhancing the accuracy of the predicted outputs.

Parametric analyses revealed that, laser powder-bed fusion parameters affect the yield and ultimate tensile strengths in a similar manner, while elongation represented a different trend as a function of all the considered input parameters. The results indicated that using high laser power, scanning speed, hatch spacing and layer thickness could have detrimental effects on tensile properties; the analysis provided an optimal range for each of the abovementioned parameters. The sensitivity analysis showed that scanning speed, laser power, hatch spacing, layer thickness and sample direction have the most significant role in variation of yield and ultimate tensile strengths, in a sequential order. However in terms of elongation, laser power was found to be the most important parameter, whereas scanning speed, hatch spacing, layer thickness and sample direction represented least influence, progressively.

Overall, the results indicate the high potential of artificial intelligence systems such as stacked auto-encoder assigned deep neural network to be used as a powerful alternative tool for parametric analysis and optimization of different additive manufacturing technologies such as laser powder-bed fusion with very high accuracy. These approaches can be sourced to efficiently tune the process parameters based on the target mechanical properties.

Declaration

Conflict of interest The authors declared no conflict of interest.

References

Aboulkhair, N.T., Everitt, N.M., Ashcroft, I., Tuck, C.: Reducing porosity in AlSi10Mg parts processed by selective laser melting. Addit. Manuf. (2014). https://doi.org/10.1016/j.addma.2014.08.001

Aboutaleb, A.M., Mahtabi, M.J., Tschopp, M.A., Bian, L.: Multi-objective accelerated process optimization of mechanical properties in laser-based additive manufacturing: Case study on Selective Laser Melting (SLM) Ti-6Al-4V. J. Manuf. Process. **38**, 432–444 (2019). https://doi.org/10.1016/j.jmapro.2018.12.040

Aggarangsi, P., Beuth, J.L.: Localized preheating approaches for reducing residual stress in additive manufacturing, in: 17th Solid Free. Fabr. Symp. SFF 2006, 2006.

Alfaify, A.Y., Hughes, J., Ridgway, K.: Critical evaluation of the pulsed selective laser melting process when fabricating Ti64 parts using a range of particle size distributions. Addit. Manuf. (2018). https://doi.org/10.1016/j.addma.2017.12.003

ASTM International, F2792–12a—Standard Terminology for Additive Manufacturing Technologies, 2013. https://doi.org/10.1520/F2792-12A.2.

Averyanova, M., Cicala, E., Bertrand, P., Grevey, D.: Experimental design approach to optimize selective laser melting of martensitic 17–4 PH powder: Part i - Single laser tracks and first layer. Rapid Prototyp. J. **18**, 28–37 (2012). https://doi.org/10.1108/13552541211193476

Bagherifard, S., Guagliano, M.: Fatigue performance of cold spray deposits: Coating, repair and additive manufacturing cases. Int. J. Fatigue. (2020). https://doi.org/10.1016/j.ijfatigue.2020.105744

Bagherifard, S., Roscioli, G., Zuccoli, M.V., Hadi, M., D'Elia, G., Demir, A.G., Previtali, B., Kondás, J., Guagliano, M.: Cold spray deposition of freestanding inconel samples and comparative analysis with selective laser melting. J. Therm. Spray Technol. (2017). https://doi.org/10.1007/s11666-017-0572-3

Bagherifard, S., Monti, S., Zuccoli, M.V., Riccio, M., Kondás, J., Guagliano, M.: Cold spray deposition for additive manufacturing of freeform structural components compared to selective laser melting. Mater. Sci. Eng. A. (2018). https://doi.org/10.1016/j.msea.2018.02.094

Bagherifard, S., Heydari Astaraee, A., Locati, M., Nawaz, A., Monti, S., Kondás, J., Singh, R., Guagliano, M.: Design and analysis of additive manufacturedbimodal structures obtained by cold spray deposition. Addit. Manuf. (2020). https://doi.org/10.1016/j.addma.2020.101131.

Bai, Y., Yang, Y., Xiao, Z., Zhang, M., Wang, D.: Process optimization and mechanical property evolution of AlSiMg0.75 by selective laser melting. Mater. Des. 140 (2018) 257–266. https://doi.org/10.1016/j.matdes.2017.11.045.

Baitimerov, R.M., Lykov, P.A., Radionova, L.V., Safonov, E.V.: Parameter optimization for selective laser melting of TiAl6V4 alloy by CO2 laser. IOP Conf. Ser. Mater. Sci. Eng. **248**, 6–11 (2017). https://doi.org/10.1088/1757-899X/248/1/012012

Bengio, Y., Lamblin, P., Popovici, D., Larochelle, H.: Greedy layer-wise training of deep networks. Adv. Neural Inf. Process. Syst. (2007). https://doi.org/10.7551/mitpress/7503.003.0024

Bin Wang, Y., You, Z.H., Li, X., Jiang, T.H., Chen, X., Zhou, X., Wang, L.: Predicting protein-protein interactions from protein sequences by a stacked sparse autoencoder deep neural network. Mol. Biosyst. (2017). https://doi.org/10.1039/c7mb00188f.

Buchbinder, D., Schleifenbaum, H., Heidrich, S., Meiners, W., Bültmann, J.: High power Selective Laser Melting (HP SLM) of aluminum parts. Phys. Procedia (2011). https://doi.org/10.1016/j.phpro.2011.03.035

Cai, C., Gao, X., Teng, Q., Li, M., Pan, K., Song, B., Yan, C., Wei, Q., Shi, Y.: A novel hybrid selective laser melting/hot isostatic pressing of near-net shaped Ti-6Al-4V alloy using an in-situ tooling: Interfacial microstructure evolution and enhanced mechanical properties. Mater. Sci. Eng. A. **717**, 95–104 (2018). https://doi.org/10.1016/j.msea.2018.01.079

Cain, V., Thijs, L., Van Humbeeck, J., Van Hooreweder, B., Knutsen, R.: Crack propagation and fracture toughness of Ti6Al4V alloy produced by selective laser melting. Addit. Manuf. (2015). https://doi.org/10.1016/j.addma.2014.12.006

Campanelli, S.L., Casalino, G., Contuzzi, N., Ludovico, A.D.: Taguchi optimization of the surface finish obtained by laser ablation on selective laser molten steel parts. Procedia CIRP. **12**, 462–467 (2013). https://doi.org/10.1016/j.procir.2013.09.079

Campoli, G., Borleffs, M.S., Amin Yavari, S., Wauthle, R., Weinans, H., Zadpoor, A.A.: Mechanical properties of open-cell metallic biomaterials manufactured using additive manufacturing. Mater. Des. (2013). https://doi.org/10.1016/j.matdes.2013.01.071.

Cao, S., Chu, R., Zhou, X., Yang, K., Jia, Q., Lim, C.V.S., Huang, A., Wu, X.: Role of martensite decomposition in tensile properties of selective laser melted Ti-6Al-4V. J. Alloys Compd. **744**, 357–363 (2018). https://doi.org/10.1016/j.jallcom.2018.02.111

Cardaropoli, F., Alfieri, V., Caiazzo, F., Sergi, V.: Dimensional analysis for the definition of the influence of process parameters in selective laser melting of Ti-6Al-4V alloy. Proc. Inst. Mech. Eng. Part B J. Eng. Manuf. 226 (2012) 1136–1142. https://doi.org/10.1177/0954405412441885.

Casalino, G., Campanelli, S.L., Contuzzi, N., Ludovico, A.D.: Experimental investigation and statistical optimisation of the selective laser melting process of a maraging steel. Opt. Laser Technol. **65**, 151–158 (2015). https://doi.org/10.1016/j.optlastec.2014.07.021

Chen, W., Thornley, L., Coe, H.G., Tonneslan, S.J., Vericella, J.J., Zhu, C., Duoss, E.B., Hunt, R.M., Wight, M.J., Apelian, D., Pascall, A.J., Kuntz, J.D., Spadaccini, C.M.: Direct metal writing: Controlling the rheology through microstructure. Appl. Phys. Lett. (2017). https://doi.org/10.1063/1.4977555

Choo, H., Sham, K.L., Bohling, J., Ngo, A., Xiao, X., Ren, Y., Depond, P.J., Matthews, M.J., Garlea, E.: Effect of laser power on defect, texture, and microstructure of a laser powder bed fusion processed 316L stainless steel. Mater. Des. (2019). https://doi.org/10.1016/j.matdes.2018.12.006

Choren, J.A., Heinrich, S.M., Silver-Thorn, M.B.: Young's modulus and volume porosity relationships for additive manufacturing applications. J. Mater. Sci. (2013). https://doi.org/10.1007/s10853-013-7237-5

Cunningham, R., Zhao, C., Parab, N., Kantzos, C., Pauza, J., Fezzaa, K., Sun, T., Rollett, A.D.: Keyhole threshold and morphology in laser melting revealed by ultrahigh-speed x-ray imaging. Science (80-.). (2019). https://doi.org/10.1126/science.aav4687.

DebRoy, T., Wei, H.L., Zuback, J.S., Mukherjee, T., Elmer, J.W., Milewski, J.O., Beese, A.M., Wilson-Heid, A., De, A., Zhang, W.: Additive manufacturing of metallic components—Process, structure and properties. Prog. Mater. Sci. (2018). https://doi.org/10.1016/j.pmatsci.2017.10.001

Ding, X., Koizumi, Y., Wei, D., Chiba, A.: Effect of process parameters on melt pool geometry and microstructure development for electron beam melting of IN718: A systematic single bead analysis study. Addit. Manuf. (2019). https://doi.org/10.1016/j.addma.2018.12.018

Dong, Z., Liu, Y., Wen, W., Ge, J., Liang, J.: Effect of hatch spacing on melt pool and as-built quality during selective laser melting of stainless steel: Modeling and experimental approaches. Materials (basel). (2018). https://doi.org/10.3390/ma12010050

Edwards, P., Ramulu, M.: Fatigue performance evaluation of selective laser melted Ti-6Al-4V. Mater. Sci. Eng. a. (2014). https://doi.org/10.1016/j.msea.2014.01.041

Fathi, P., Rafieazad, M., Duan, X., Mohammadi, M., Nasiri, A.M.: On microstructure and corrosion behaviour of AlSi10Mg alloy with low surface roughness fabricated by direct metal laser sintering. Corros. Sci. (2019). https://doi.org/10.1016/j.corsci.2019.05.032

Feng, S., Zhou, H., Dong, H.: Using deep neural network with small dataset to predict material defects. Mater. Des. **162**, 300–310 (2019). https://doi.org/10.1016/j.matdes.2018.11.060

Fergani, O., Berto, F., Welo, T., Liang, S.Y.: Analytical modelling of residual stress in additive manufacturing. Fatigue Fract. Eng. Mater. Struct. (2017). https://doi.org/10.1111/ffe.12560

Gardan, J.: Additive manufacturing technologies: State of the art and trends. Int. J. Prod. Res. (2016). https://doi.org/10.1080/00207543.2015.1115909

Garg, A., Tai, K., Savalani, M.M.: Formulation of bead width model of an SLM prototype using modified multi-gene genetic programming approach. Int. J. Adv. Manuf. Technol. **73**, 375–388 (2014). https://doi.org/10.1007/s00170-014-5820-9

Ge, W., Guo, C., Lin, F.: Effect of process parameters on microstructure of TiAl alloy produced by electron beam selective melting. Procedia Eng. (2014). https://doi.org/10.1016/j.proeng.2014.10.096

Ghelichi, R., Bagherifard, S., Mac Donald, D., Brochu, M., Jahed, H., Jodoin, B., Guagliano, M.: Fatigue strength of Al alloy cold sprayed with nanocrystalline powders. Int. J. Fatigue. (2014). https://doi.org/10.1016/j.ijfatigue.2013.09.001.

Gockel, J., Sheridan, L., Koerper, B., Whip, B.: The influence of additive manufacturing processing parameters on surface roughness and fatigue life. Int. J. Fatigue. **124**, 380–388 (2019). https://doi.org/10.1016/j.ijfatigue.2019.03.025

Gong, H., Rafi, K., Gu, H., Janaki Ram, G.D., Starr, T., Stucker, B.: Influence of defects on mechanical properties of Ti-6Al-4V components produced by selective laser melting and electron beam melting. Mater. Des. 86 (2015) 545–554. https://doi.org/10.1016/j.matdes.2015.07.147.

Gu, D.D., Meiners, W., Wissenbach, K., Poprawe, R.: Laser additive manufacturing of metallic components: Materials, processes and mechanisms. Int. Mater. Rev. (2012). https://doi.org/10.1179/1743280411Y.0000000014

Guan, K., Wang, Z., Gao, M., Li, X., Zeng, X.: Effects of processing parameters on tensile properties of selective laser melted 304 stainless steel. Mater. Des. (2013). https://doi.org/10.1016/j.matdes.2013.03.056

Hassanin, H., Modica, F., El-Sayed, M.A., Liu, J., Essa, K.: Manufacturing of Ti–6Al–4V Micro-Implantable Parts Using Hybrid Selective Laser Melting and Micro-Electrical Discharge Machining. Adv. Eng. Mater. **18**, 1544–1549 (2016). https://doi.org/10.1002/adem.201600172

He, J., Li, D., Jiang, W., Ke, L., Qin, G., Ye, Y., Qin, Q., Qiu, D.: The Martensitic Transformation and Mechanical Properties of Ti6Al4V Prepared via Selective Laser Melting. Materials (Basel). 12 (2019). https://doi.org/10.3390/ma12020321.

Hinton, G.E., Osindero, S., Teh, Y.W.: A fast learning algorithm for deep belief nets. Neural Comput. (2006). https://doi.org/10.1162/neco.2006.18.7.1527

Hinton, G.E., Salakhutdinov, R.R.: Reducing the dimensionality of data with neural networks. Science (80-.). (2006). https://doi.org/10.1126/science.1127647.

Kempen, K., Thijs, L., Yasa, E., Badrossamay, M., Verheecke, W., Kruth, J.P.: Process optimization and microstructural analysis for selective laser melting of AlSi10Mg. In: 22nd Annu. Int. Solid Free. Fabr. Symp. - An Addit. Manuf. Conf. SFF 2011. (2011) 484–495.

Khaimovich, A.I., Stepanenko, I.S., Smelov, V.G.: Optimization of Selective Laser Melting by Evaluation Method of Multiple Quality Characteristics. IOP Conf. Ser. Mater. Sci. Eng. 302 (2018). https://doi.org/10.1088/1757-899X/302/1/012067.

Kumar, S., Czekanski, A.: Optimization of parameters for SLS of WC-Co. Rapid Prototyp. J. (2017). https://doi.org/10.1108/RPJ-10-2016-0168

Kwon, O., Kim, H.G., Ham, M.J., Kim, W., Kim, G.H., Cho, J.H., Il Kim, N., Kim, K.: A deep neural network for classification of melt-pool images in metal additive manufacturing. J. Intell. Manuf. 31 (2018) 375–386. https://doi.org/10.1007/s10845-018-1451-6.

Le, K.Q., Tang, C., Wong, C.H.: On the study of keyhole-mode melting in selective laser melting process. Int. J. Therm. Sci. (2019). https://doi.org/10.1016/j.ijthermalsci.2019.105992

Liberini, M., Astarita, A., Campatelli, G., Scippa, A., Montevecchi, F., Venturini, G., Durante, M., Boccarusso, L., Minutolo, F.M.C., Squillace, A.: Selection of optimal process parameters for wire arc additive manufacturing. Procedia CIRP. **62**, 470–474 (2017). https://doi.org/10.1016/j.procir.2016.06.124

Liu, C., Zhang, M., Chen, C.: Effect of laser processing parameters on porosity, microstructure and mechanical properties of porous Mg-Ca alloys produced by laser additive manufacturing. Mater. Sci. Eng. a. **703**, 359–371 (2017). https://doi.org/10.1016/j.msea.2017.07.031

Liu, G., Bao, H., Han, B.: A stacked autoencoder-based deep neural network for achieving Gearbox fault diagnosis. Math. Probl. Eng. (2018). https://doi.org/10.1155/2018/5105709

Livingstone, D.J., Manallack, D.T., Tetko, I.V.: Data modelling with neural networks: Advantages and limitations. J. Comput. Aided. Mol. Des. (1997). https://doi.org/10.1023/A:1008074223811

Ma, M., Wang, Z., Gao, M., Zeng, X.: Layer thickness dependence of performance in high-power selective laser melting of 1Cr18Ni9Ti stainless steel. J. Mater. Process. Technol. **215**, 142–150 (2015). https://doi.org/10.1016/j.jmatprotec.2014.07.034

Ma, Z., Zhang, K., Ren, Z., Zhang, D.Z., Tao, G., Xu, H.: Selective laser melting of Cu–Cr–Zr copper alloy: Parameter optimization, microstructure and mechanical properties. J. Alloys Compd. (2020). https://doi.org/10.1016/j.jallcom.2020.154350

Maizza, G., Caporale, A., Polley, C., Seitz, H.: Micro-macro relationship between microstructure, porosity, mechanical properties, and build mode parameters of a selective-electron-beam-melted ti-6al-4v alloy. Metals (Basel). 9 (2019). https://doi.org/10.3390/met9070786.

Maleki, N., Maleki, E.: Modeling of cathode Pt /C electrocatalyst degradation and performance of a PEMFC using artificial neural network. ACM Int. Conf. Proceeding Ser. (2015). https://doi.org/10.1145/2832987.2833000

Maleki, E., Unal, O.: Shot Peening Process Effects on Metallurgical and Mechanical Properties of 316 L Steel via: Experimental and Neural Network Modeling. Met. Mater. Int. (2019). https://doi.org/10.1007/s12540-019-00448-3

Maleki, E., Unal, O.: Optimization of shot peening effective parameters on surface hardness improvement. Met. Mater. Int. (2020a). https://doi.org/10.1007/s12540-020-00758-x

Maleki, E., Unal, O.: Fatigue limit prediction and analysis of nano-structured AISI 304 steel by severe shot peening via ANN. Eng. Comput. (2020b). https://doi.org/10.1007/s00366-020-00964-6

Maleki, N., Kashanian, S., Maleki, E., Nazari, M.: A novel enzyme based biosensor for catechol detection in water samples using artificial neural network. Biochem. Eng. J. **128**, 1–11 (2017). https://doi.org/10.1016/j.bej.2017.09.005

Maleki, E., Bagherifard, S., Bandini, M., Guagliano, M.: Surface post-treatments for metal additive manufacturing: Progress, challenges, and opportunities. Addit. Manuf. (2020a). https://doi.org/10.1016/j.addma.2020.101619

Maleki, E., Mirzaali, M.J., Guagliano, M., Bagherifard, S.: Analyzing the mechano-bactericidal effect of nano-patterned surfaces on different bacteria species. Surf. Coatings Technol. (2020b). https://doi.org/10.1016/j.surfcoat.2020.126782

Maleki, E., Unal, O., Guagliano, M., Bagherifard, S.: Analysing the fatigue behaviour and residual stress relaxation of gradient nano-structured 316L Steel subjected to the shot peening via deep learning approach. Met. Mater. Int. (2021). https://doi.org/10.1007/s12540-021-00995-8

Maleki, E., Farrahi, G.H.H.: Modelling of conventional and severe shot peening influence on properties of high carbon steel via artificial neural network.Int. J. Eng. Trans. B Appl. 31 (2018). https://doi.org/10.5829/ije.2017.30.11b.00.

Maleki, E., Unal, O., Reza Kashyzadeh, K.: Fatigue behavior prediction and analysis of shot peened mild carbon steels. Int. J. Fatigue. 116 (2018) 48–67. https://doi.org/10.1016/j.ijfatigue.2018.06.004.

Maleki, E., Unal, O., Reza Kashyzadeh, K.: Surface layer nanocrystallization of carbon steels subjected to severe shot peening: Analysis and optimization. Mater. Charact. (2019). https://doi.org/10.1016/j.matchar.2019.109877.

Malỳ, M., Höller, C., Skalon, M., Meier, B., Koutnỳ, D., Pichler, R., Sommitsch, C., Paloušek, D.: Effect of process parameters and high-temperature preheating on residual stress and relative density of Ti6Al4V processed by selective laser melting, Materials (Basel). 16 (2019). https://doi.org/10.3390/ma12060930.

Manjunath, A., Anandakrishnan, V., Ramachandra, S., Parthiban, K.: Experimental investigations on the effect of pre-positioned wire electron beam additive manufacturing process parameters on the layer geometry of titanium 6Al4V. Mater. Today Proc. (2020). https://doi.org/10.1016/j.matpr.2019.06.755

Marrey, M., Malekipour, E., El-Mounayri, H., Faierson, E.J.: A framework for optimizing process parameters in powder bed fusion (PBF) process using artificial neural network (ANN). Procedia Manuf. **34**, 505–515 (2019). https://doi.org/10.1016/j.promfg.2019.06.214

Matthews, M.J., Guss, G., Drachenberg, D.R., Demuth, J.A., Heebner, J.E., Duoss, E.B., Kuntz, J.D., Spadaccini, C.M.: Diode-based additive manufacturing of metals using an optically-addressable light valve. Opt. Express. (2017). https://doi.org/10.1364/oe.25.011788

Meier, C., Penny, R.W., Zou, Y., Gibbs, J.S., Hart, A.J.: Thermophysical phenomena in metal additive manufacturing by selective laser melting: fundamentals, modeling, simulation, and experimentation. Annu. Rev. Heat Transf. **20**, 241–316 (2018). https://doi.org/10.1615/annualrevheattransfer.2018019042

Mertens, A., Reginster, S., Paydas, H., Contrepois, Q., Dormal, T., Lemaire, O., Lecomte-Beckers, J.: Mechanical properties of alloy Ti-6Al-4V and of stainless steel 316L processed by selective laser melting: Influence of out-of-equilibrium microstructures. Powder Metall. **57**, 184–189 (2014). https://doi.org/10.1179/1743290114Y.0000000092

Moussaoui, K., Rubio, W., Mousseigne, M., Sultan, T., Rezai, F.: Effects of Selective Laser Melting additive manufacturing parameters of Inconel 718 on porosity, microstructure and mechanical properties. Mater. Sci. Eng. a. **735**, 182–190 (2018). https://doi.org/10.1016/j.msea.2018.08.037

Mozaffar, M., Paul, A., Al-Bahrani, R., Wolff, S., Choudhary, A., Agrawal, A., Ehmann, K., Cao, J.: Data-driven prediction of the high-dimensional thermal history in directed energy deposition processes via recurrent neural networks. Manuf. Lett. **18**, 35–39 (2018). https://doi.org/10.1016/j.mfglet.2018.10.002

Mutua, J., Nakata, S., Onda, T., Chen, Z.C.: Optimization of selective laser melting parameters and influence of post heat treatment on microstructure and mechanical properties of maraging steel. Mater. Des. **139**, 486–497 (2018). https://doi.org/10.1016/j.matdes.2017.11.042

Nasab, M.H., Gastaldi, D., Lecis, N.F., Vedani, M.: On morphological surface features of the parts printed by selective laser melting (SLM). Addit. Manuf. (2018). https://doi.org/10.1016/j.addma.2018.10.011

Olakanmi, E.O., Cochrane, R.F., Dalgarno, K.W.: A review on selective laser sintering/melting (SLS/SLM) of aluminium alloy powders: Processing, microstructure, and properties. Prog. Mater. Sci. **74**, 401–477 (2015). https://doi.org/10.1016/j.pmatsci.2015.03.002

Olden, J.D., Joy, M.K., Death, R.G.: An accurate comparison of methods for quantifying variable importance in artificial neural networks using simulated data. Ecol. Modell. (2004). https://doi.org/10.1016/j.ecolmodel.2004.03.013

Pang, Z., Liu, Y., Li, M., Zhu, C., Li, S., Wang, Y., Wang, D., Song, C.: Influence of process parameter and strain rate on the dynamic compressive properties of selective laser-melted Ti-6Al-4V alloy. Appl. Phys. A Mater. Sci. Process. **125**, 1–12 (2019). https://doi.org/10.1007/s00339-018-2359-x

Paul, R., Anand, S.: Process energy analysis and optimization in selective laser sintering. J. Manuf. Syst. **31**, 429–437 (2012). https://doi.org/10.1016/j.jmsy.2012.07.004

Qiu, C., Adkins, N.J.E., Attallah, M.M.: Microstructure and tensile properties of selectively laser-melted and of HIPed laser-melted Ti-6Al-4V. Mater. Sci. Eng. a. **578**, 230–239 (2013). https://doi.org/10.1016/j.msea.2013.04.099

Qiu, C., Panwisawas, C., Ward, M., Basoalto, H.C., Brooks, J.W., Attallah, M.M.: On the role of melt flow into the surface structure and porosity development during selective laser melting. Acta Mater. **96**, 72–79 (2015). https://doi.org/10.1016/j.actamat.2015.06.004

Raghavan, N., Dehoff, R., Pannala, S., Simunovic, S., Kirka, M., Turner, J., Carlson, N., Babu, S.S.: Numerical modeling of heat-transfer and the influence of process parameters on tailoring the grain morphology of IN718 in electron beam additive manufacturing. Acta Mater. (2016). https://doi.org/10.1016/j.actamat.2016.03.063

Riquelme, A., Rodrigo, P., Escalera-Rodriguez, M.D., Rams, J.: Effect of the process parameters in the additive manufacturing of in situ Al/AlN samples. J. Manuf. Process. **46**, 271–278 (2019). https://doi.org/10.1016/j.jmapro.2019.09.011

Sames, W.J., List, F.A., Pannala, S., Dehoff, R.R., Babu, S.S.: The metallurgy and processing science of metal additive manufacturing. Int. Mater. Rev. (2016). https://doi.org/10.1080/09506608.2015.1116649

Saqiba, S., Urbanica, R.J., Aggarwal, K.: Analysis of laser cladding bead morphology for developing additive manufacturing travel paths. Procedia CIRP. **17**, 824–829 (2014). https://doi.org/10.1016/j.procir.2014.01.098

Schnabel, K., Baumgartner, J., Möller, B.: Fatigue assessment of additively manufactured metallic structures using local approaches based on finite-element simulations. Procedia Struct. Integr. (2019). https://doi.org/10.1016/j.prostr.2019.12.048

Scime, L., Beuth, J.: A multi-scale convolutional neural network for autonomous anomaly detection and classification in a laser powder bed fusion additive manufacturing process. Addit. Manuf. **24**, 273–286 (2018). https://doi.org/10.1016/j.addma.2018.09.034

Sharma, A., Bandari, V., Ito, K., Kohama, K., Ramji, R.M., Himasekhar, H.S.: A new process for design and manufacture of tailor-made functionally graded composites through friction stir additive manufacturing. J. Manuf. Process. (2017). https://doi.org/10.1016/j.jmapro.2017.02.007

Shi, X., Ma, S., Liu, C., Wu, Q., Lu, J., Liu, Y., Shi, W.: Selective laser melting-wire arc additive manufacturing hybrid fabrication of Ti-6Al-4V alloy: Microstructure and mechanical properties. Mater. Sci. Eng. a. **684**, 196–204 (2017). https://doi.org/10.1016/j.msea.2016.12.065

Shi, W., Liu, y., Shi, X., Hou, Y., Wang, P., Song, G.: Beam diameter dependence of performance in thick-layer and high-power selective laser melting of Ti-6Al-4V. Materials (Basel). 11 (2018). https://doi.org/10.3390/ma11071237.

Simonelli, M., Tse, Y.Y., Tuck, C.: Effect of the build orientation on the mechanical properties and fracture modes of SLM Ti-6Al-4V. Mater. Sci. Eng. a. (2014). https://doi.org/10.1016/j.msea.2014.07.086

Spierings, A.B., Herres, N., Levy, G.: Influence of the particle size distribution on surface quality and mechanical properties in AM steel parts. Rapid Prototyp. J. (2011). https://doi.org/10.1108/13552541111124770

Stef, J., Poulon-Quintin, A., Redjaimia, A., Ghanbaja, J., Ferry, O., De Sousa, M., Gouné, M.: Mechanism of porosity formation and influence on mechanical properties in selective laser melting of Ti-6Al-4V parts. Mater. Des. **156**, 480–493 (2018). https://doi.org/10.1016/j.matdes.2018.06.049

Stender, M.E., Beghini, L.L., Sugar, J.D., Veilleux, M.G., Subia, S.R., Smith, T.R., Marchi, C.W.S., Brown, A.A., Dagel, D.J.: A thermal-mechanical finite element workflow for directed energy deposition additive manufacturing process modeling. Addit. Manuf. (2018). https://doi.org/10.1016/j.addma.2018.04.012

Su, X., Yang, Y.: Research on track overlapping during Selective Laser Melting of powders. J. Mater. Process. Technol. (2012). https://doi.org/10.1016/j.jmatprotec.2012.05.012

Sui, Q., Li, P., Wang, K., Yin, X., Liu, L., Zhang, Y., Zhang, Q., Wang, S., Wang, L.: Effect of build orientation on the corrosion behavior and mechanical properties of selective laser melted Ti-6Al-4V. Metals (Basel). 9 (2019). https://doi.org/10.3390/met9090976.

Sun, J., Yang, Y., Wang, D.: Parametric optimization of selective laser melting for forming Ti6Al4V samples by Taguchi method. Opt. Laser Technol. **49**, 118–124 (2013). https://doi.org/10.1016/j.optlastec.2012.12.002

Sun, Z., Tan, X., Tor, S.B., Yeong, W.Y.: Selective laser melting of stainless steel 316L with low porosity and high build rates. Mater. Des. (2016). https://doi.org/10.1016/j.matdes.2016.05.035

Sun, D., Gu, D., Lin, K., Ma, J., Chen, W., Huang, J., Sun, X., Chu, M.: Selective laser melting of titanium parts: Influence of laser process parameters on macro- and microstructures and tensile property. Powder Technol. (2019). https://doi.org/10.1016/j.powtec.2018.09.090

Sun, X., Liu, D., Zhou, W., Nomura, N., Tsutsumi, Y., Hanawa, T.: Effects of process parameters on the mechanical properties of additively manufactured Zr–1Mo alloy builds. J. Mech. Behav. Biomed. Mater. **104**, 103655 (2020). https://doi.org/10.1016/j.jmbbm.2020.103655

Tao, P., Xue Li, H., ying Huang, Y., dong Hu, Q., li Gong, S., yan Xu, Q.: Tensile behavior of Ti-6Al-4V alloy fabricated by selective laser melting: effects of microstructures and as-built surface qualit. China Foundry. 15 (2018) 243–252. https://doi.org/10.1007/s41230-018-8064-8.

Te Liao, H., Shie, J.R.: Optimization on selective laser sintering of metallic powder via design of experiments method. Rapid Prototyp. J. **13**, 156–162 (2007). https://doi.org/10.1108/13552540710750906

Tetko, I. V., Livingstone, D.J., Luik, A.I.: Neural Network Studies. 1. Comparison of Overfitting and Overtraining. J. Chem. Inf. Comput. Sci. (1995). https://doi.org/10.1021/ci00027a006.

Thijs, L., Verhaeghe, F., Craeghs, T., Van Humbeeck, J., Kruth, J.P.: A study of the microstructural evolution during selective laser melting of Ti-6Al-4V. Acta Mater. **58**, 3303–3312 (2010). https://doi.org/10.1016/j.actamat.2010.02.004

Thompson, S.M., Bian, L., Shamsaei, N., Yadollahi, A.: An overview of Direct Laser Deposition for additive manufacturing; Part I: Transport phenomena, modeling and diagnostics. Addit. Manuf. (2015). https://doi.org/10.1016/j.addma.2015.07.001

Tonelli, L., Fortunato, A., Ceschini, L.: CoCr alloy processed by Selective Laser Melting (SLM): effect of Laser Energy Density on microstructure, surface morphology, and hardness. J. Manuf. Process. **52**, 106–119 (2020). https://doi.org/10.1016/j.jmapro.2020.01.052

Tran, H.C., Lo, Y.L.: Heat transfer simulations of selective laser melting process based on volumetric heat source with powder size consideration. J. Mater. Process. Technol. (2018). https://doi.org/10.1016/j.jmatprotec.2017.12.024

Tran, H.C., Lo, Y.L.: Systematic approach for determining optimal processing parameters to produce parts with high density in selective laser melting process. Int. J. Adv. Manuf. Technol. (2019). https://doi.org/10.1007/s00170-019-04517-0

Vilaro, T., Colin, C., Bartout, J.D.: As-fabricated and heat-treated microstructures of the Ti-6Al-4V alloy processed by selective laser melting. Metall. Mater. Trans. A Phys. Metall. Mater. Sci. 42 (2011) 3190–3199. https://doi.org/10.1007/s11661-011-0731-y.

Voisin, T., Calta, N.P., Khairallah, S.A., Forien, J.B., Balogh, L., Cunningham, R.W., Rollett, A.D., Wang, Y.M.: Defects-dictated tensile properties of selective laser melted Ti-6Al-4V. Mater. Des. **158**, 113–126 (2018). https://doi.org/10.1016/j.matdes.2018.08.004

Wang, Z., Palmer, T.A., Beese, A.M.: Effect of processing parameters on microstructure and tensile properties of austenitic stainless steel 304L made by directed energy deposition additive manufacturing. Acta Mater. **110**, 226–235 (2016). https://doi.org/10.1016/j.actamat.2016.03.019

Wang, C., Tan, X., Liu, E., Tor, S.B.: Process parameter optimization and mechanical properties for additively manufactured stainless steel 316L parts by selective electron beam melting. Mater. Des. (2018). https://doi.org/10.1016/j.matdes.2018.03.035

Wang, C., Tan, X.P., Du, Z., Chandra, S., Sun, Z., Lim, C.W.J., Tor, S.B., Lim, C.S., Wong, C.H.: Additive manufacturing of NiTi shape memory alloys using pre-mixed powders. J. Mater. Process. Technol. (2019). https://doi.org/10.1016/j.jmatprotec.2019.03.025

Wang, C., Tan, X.P., Tor, S.B., Lim, C.S.: Machine learning in additive manufacturing: State-of-the-art and perspectives. Addit. Manuf. (2020a). https://doi.org/10.1016/j.addma.2020.101538

Wang, D., Ye, G., Dou, W., Zhang, M., Yang, Y., Mai, S., Liu, Y.: Influence of spatter particles contamination on densification behavior and tensile properties of CoCrW manufactured by selective laser melting. Opt. Laser Technol. (2020b). https://doi.org/10.1016/j.optlastec.2019.105678

Wołosz, P., Baran, A., Polański, M.: The influence of laser engineered net shaping (LENS^{TM}) technological parameters on the laser deposition efficiency and properties of H13 (AISI) steel. J. Alloys Compd. (2020). https://doi.org/10.1016/j.jallcom.2020.153840

Wu, M.W., Lai, P.H., Chen, J.K.: Anisotropy in the impact toughness of selective laser melted Ti-6Al-4V alloy. Mater. Sci. Eng. a. **650**, 295–299 (2016). https://doi.org/10.1016/j.msea.2015.10.045

Xia, M., Gu, D., Yu, G., Dai, D., Chen, H., Shi, Q.: Influence of hatch spacing on heat and mass transfer, thermodynamics and laser processability during additive manufacturing of Inconel 718 alloy. Int. J. Mach. Tools Manuf. (2016). https://doi.org/10.1016/j.ijmachtools.2016.07.010

Xiong, J., Zhang, G., Hu, J., Wu, L.: Bead geometry prediction for robotic GMAW-based rapid manufacturing through a neural network and a second-order regression analysis. J. Intell. Manuf. (2014). https://doi.org/10.1007/s10845-012-0682-1

Xiong, J., Li, Y., Li, R., Yin, Z.: Influences of process parameters on surface roughness of multi-layer single-pass thin-walled parts in GMAW-based additive manufacturing. J. Mater. Process. Technol. **252**, 128–136 (2018). https://doi.org/10.1016/j.jmatprotec.2017.09.020

Xu, W., Brandt, M., Sun, S., Elambasseril, J., Liu, Q., Latham, K., Xia, K., Qian, M.: Additive manufacturing of strong and ductile Ti-6Al-4V by selective laser melting via in situ martensite decomposition. Acta Mater. **85**, 74–84 (2015). https://doi.org/10.1016/j.actamat.2014.11.028

Yadollahi, A., Shamsaei, N.: Additive manufacturing of fatigue resistant materials: Challenges and opportunities. Int. J. Fatigue. (2017). https://doi.org/10.1016/j.ijfatigue.2017.01.001

Yadroitsev, I., Smurov, I.: Surface morphology in selective laser melting of metal powders. Phys. Procedia (2011). https://doi.org/10.1016/j.phpro.2011.03.034

Yakout, M., Cadamuro, A., Elbestawi, M.A., Veldhuis, S.C.: The selection of process parameters in additive manufacturing for aerospace alloys. Int. J. Adv. Manuf. Technol. (2017). https://doi.org/10.1007/s00170-017-0280-7

Yakout, M., Elbestawi, M.A., Veldhuis, S.C.: On the characterization of stainless steel 316L parts produced by selective laser melting. Int. J. Adv. Manuf. Technol. (2018). https://doi.org/10.1007/s00170-017-1303-0

Yakout, M., Elbestawi, M.A., Veldhuis, S.C.: Density and mechanical properties in selective laser melting of Invar 36 and stainless steel 316L. J. Mater. Process. Technol. (2019). https://doi.org/10.1016/j.jmatprotec.2018.11.006

Yan, Y., Geng, W., Qiu, J., Ke, H., Luo, C., Yang, J., Uher, C., Tang, X.: Thermoelectric properties of n-type ZrNiSn prepared by rapid non-equilibrium laser processing. RSC Adv. (2018). https://doi.org/10.1039/c8ra00992a

Yang, J., Han, J., Yu, H., Yin, J., Gao, M., Wang, Z., Zeng, X.: Role of molten pool mode on formability, microstructure and mechanical properties of selective laser melted Ti-6Al-4V alloy. Mater. Des. **110**, 558–570 (2016). https://doi.org/10.1016/j.matdes.2016.08.036

Yang, G., Yang, P., Yang, K., Liu, N., Jia, L., Wang, J., Tang, H.: Effect of processing parameters on the density, microstructure and strength of pure tungsten fabricated by selective electron beam melting. Int. J. Refract. Met. Hard Mater. (2019a). https://doi.org/10.1016/j.ijrmhm.2019.105040

Yang, T., Liu, T., Liao, W., MacDonald, E., Wei, H., Chen, X., Jiang, L.: The influence of process parameters on vertical surface roughness of the AlSi10Mg parts fabricated by selective laser melting. J. Mater. Process. Technol. (2019b). https://doi.org/10.1016/j.jmatprotec.2018.10.015

Yang, L., Zhicong, P., Ming, L., Yonggang, W., Di, W., Changhui, S., Shuxin, L.: Investigation into the dynamic mechanical properties of selective laser melted Ti-6Al-4V alloy at high strain rate tensile loading. Mater. Sci. Eng. a. **745**, 440–449 (2019c). https://doi.org/10.1016/j.msea.2019.01.010

Yang, Y., liu, Y.J., Chen, J., Wang, H.L., Zhang, Z.Q., Lu, Y.J., Wu, S.Q., Lin, J.X.: Crystallographic features of α variants and β phase for Ti-6Al-4V alloy fabricated by selective laser melting. Mater. Sci. Eng. A. 707 (2017) 548–558. https://doi.org/10.1016/j.msea.2017.09.068.

Yu, H., Yang, J., Yin, J., Wang, Z., Zeng, X.: Comparison on mechanical anisotropies of selective laser melted Ti-6Al-4V alloy and 304 stainless steel. Mater. Sci. Eng. a. **695**, 92–100 (2017). https://doi.org/10.1016/j.msea.2017.04.031

Zafari, A., Barati, M.R., Xia, K.: Controlling martensitic decomposition during selective laser melting to achieve best ductility in high strength Ti-6Al-4V. Mater. Sci. Eng. a. **744**, 445–455 (2019). https://doi.org/10.1016/j.msea.2018.12.047

Zhang, B., Dembinski, L., Coddet, C.: The study of the laser parameters and environment variables effect on mechanical properties of high compact parts elaborated by selective laser melting 316L powder. Mater. Sci. Eng. a. (2013). https://doi.org/10.1016/j.msea.2013.06.055

Zhang, P., Zhang, D.Z., Peng, D., Li, Z., Mao, Z.: Rolling contact fatigue performance evaluation of Ti–6Al–4V parts processed by selective laser melting. Int. J. Adv. Manuf. Technol. **96**, 3533–3543 (2018). https://doi.org/10.1007/s00170-018-1576-y

Zhang, S., Rauniyar, S., Shrestha, S., Ward, A., Chou, K.: An experimental study of tensile property variability in selective laser melting. J. Manuf. Process. (2019a). https://doi.org/10.1016/j.jmapro.2019.03.045

Zhang, B., Liu, S., Shin, Y.C.: In-Process monitoring of porosity during laser additive manufacturing process. Addit. Manuf. (2019b). https://doi.org/10.1016/j.addma.2019.05.030

Zhang, H., Dong, D., Su, S., Chen, A.: Experimental study of effect of post processing on fracture toughness and fatigue crack growth performance of selective laser melting Ti-6Al-4V. Chinese J. Aeronaut. **32**, 2383–2393 (2019c). https://doi.org/10.1016/j.cja.2018.12.007

Zhao, X., Li, S., Zhang, M., Liu, Y., Sercombe, T.B., Wang, S., Hao, Y., Yang, R., Murr, L.E.: Comparison of the microstructures and mechanical properties of Ti-6Al-4V fabricated by selective laser melting and electron beam melting. Mater. Des. **95**, 21–31 (2016). https://doi.org/10.1016/j.matdes.2015.12.135

Zhao, J.R., Hung, F.Y., Lui, T.S., Wu, Y.L.: The relationship of fracture mechanism between high temperature tensile mechanical properties and particle erosion resistance of selective laser melting Ti-6al-4v alloy. Metals (Basel). 9 (2019). https://doi.org/10.3390/met9050501.

Zheng, M., Wei, L., Chen, J., Zhang, Q., Li, J., Sui, S., Wang, G., Huang, W.: Surface morphology evolution during pulsed selective laser melting: Numerical and experimental investigations. Appl. Surf. Sci. (2019). https://doi.org/10.1016/j.apsusc.2019.143649